Journal of Geophysical Research: Atmospheres

RESEARCH ARTICLE
10.1029/2018JD028350

Assessment of Regional Mercury Deposition and Emission Outflow in Mainland China

Xun Wang[1], Che-Jen Lin[1,3,4], Xinbin Feng[1], Wei Yuan[1,2], Xuewu Fu[1], Hui Zhang[1], Qingru Wu[5,6], and Shuxiao Wang[5,6]

[1]State Key Laboratory of Environmental Geochemistry, Institute of Geochemistry, Chinese Academy of Sciences, Guiyang, China, [2]University of Chinese Academy of Sciences, Huairou, China, [3]Center for Advances in Water and Air Quality, Lamar University, Beaumont, TX, USA, [4]Department of Civil and Environmental Engineering, Lamar University, Beaumont, TX, USA, [5]State Key Joint Laboratory of Environmental Simulation and Pollution Control, School of Environment, Tsinghua University, Beijing, China, [6]State Environmental Protection Key Laboratory of Sources and Control of Air Pollution Complex, Beijing, China

Abstract Mainland China is the largest emission region of anthropogenic mercury (Hg) in the world. There have been concerns regarding the emission outflow and chemical transport budget of Hg in the region. Earlier assessments of Hg chemical transport were based on relatively outdated emission data. Recent estimates for anthropogenic (Wu et al., 2016, https://doi.org/10.1021/acs.est.6b04308) and natural Hg emissions (X. Wang, Lin, et al., 2016, https://doi.org/10.5194/acp-16-11125-2016) show substantial differences from earlier emission inventories. In this study, we applied the updated Hg emission estimates to reassess the regional transport budget using Community Multiscale Air Quality-Hg v5.1. Our results show that the variation of simulated concentration, deposition, and associated emission outflow of Hg are primarily influenced by the spatial-temporal variation of Hg emissions, monsoon shifts, and particulate matter pollution in China. Total Hg deposition in Mainland China is estimated to be 422 Mg/year, and approximately two thirds of the deposition is contributed by domestic emissions. The net Hg transport budget from Mainland China is 511 Mg/year, contributing to 10% of Hg deposition in other regions of the world. This reassessment points to a ~25% reduction in total annual outflow compared to the previous estimate by Lin et al. (2010, https://doi.org/10.5194/acp-10-1853-2010). Such reduction is mainly caused by changes in Hg emission quantity, speciation, and spatial/temporal distributions. More modeling studies focusing on reducing uncertainties of emission inventories and Hg atmospheric chemistry are needed for continuous assessment of Hg emission outflow in this emission-intensive region.

Key Points:
- Recent changes in emission inventories have significant influences on atmospheric mercury outflow from China
- Total mercury deposition in China is 422 Mg/year, about two thirds of deposition is contributed by domestic emissions
- Elevated levels of aerosol and secondary air pollutants significantly enhance atmospheric mercury pollution

Supporting Information:
- Supporting Information S1

Correspondence to:
Che-JenLin and X. Feng,
fengxinbin@vip.skleg.cn;
jerry.lin@lamar.edu

Citation:
Wang, X., Lin, C.-J., Feng, X., Yuan, W., Fu, X., Zhang, H., et al. (2018). Assessment of regional mercury deposition and emission outflow in Mainland China. *Journal of Geophysical Research: Atmospheres*, *123*, 9868–9890. https://doi.org/10.1029/2018JD028350

Received 19 JAN 2018
Accepted 26 JUL 2018
Accepted article online 5 AUG 2018
Published online 12 SEP 2018

1. Introduction

Mercury (Hg) is a toxic pollutant subject to long-range transport in the atmosphere due to its relatively long atmospheric lifetime (0.5–2 years) as gaseous elemental mercury (GEM; Lin et al., 2010; Selin, 2009). In addition to GEM, atmospheric Hg also exists in two operationally defined species: gaseous oxidized mercury (GOM) and particulate bound mercury (PBM). Both GOM and PBM (<5% total atmospheric Hg) have much shorter residence time (few days to weeks) and tend to deposit locally through wet and dry deposition (Lindberg et al., 2007; Selin, 2009). Once deposited, Hg methylation and bioaccumulation of methylated Hg in the food chain pose a threat to ecosystems and human health. Methylated Hg pollution in fish and rice has been a public health concern worldwide (Driscoll et al., 1994; P. Li et al., 2017).

To alleviate the impact of global Hg pollution, international efforts to curb manmade Hg emissions have culminated in the 2013 legally binding *Minamata Convention on Mercury*. Anthropogenic emission sources release Hg^0, Hg^{2+}, and particle Hg (Hg_P), while natural sources release Hg^0 only. The so-called *natural emission* in this study refers to the Hg release associated with natural processes emitting Hg^0 from the natural surfaces including soil, water, vegetation, ice, and snow surfaces, including re-emission of previously deposited Hg. Hg emissions and their outflow from East Asia have been regarded as a concern to global Hg pollution due to the large quantity of Hg release in the region (L. Chen et al., 2014; Jaffe et al., 2005; Lin et al., 2010). According to the 2013 Global Mercury Assessment, anthropogenic Hg emissions in East Asia account for 35% of global total in 2010 (UNEP, 2013), with China as the largest emitter (De Simone et al., 2016). Accurate emission inventories are the foundation for assessing the Hg emission outflow in China.

The continued economic growth and improved air pollution control in China have greatly changed the anthropogenic Hg emission and speciation in recent years (Y. X. Zhang, Jacob, et al., 2016). As more-reliable emission data become available, reassessment of the regional Hg chemical transport and emission outflow using the updated emission data is necessary. Recent studies on anthropogenic Hg emissions suggest that (1) atmospheric Hg emission in China peaked in 2011 at 565 Mg/year and then dropped to 530 Mg/year in 2014 (Wu et al., 2016), and (2) emission speciation gradually shifted to a larger fraction of oxidized Hg (51/46/3 for $Hg^0/Hg^{2+}/Hg_P$ in 2014; Wu et al., 2016; L Zhang, Wang, et al., 2015; Zhao et al., 2015). Compared to the speciation form in *GMP 2013* (GMP: Global Mercury Partnership; 80/16/4 for $Hg^0/Hg^{2+}/Hg_P$; UNEP, 2013), such an emission speciation shift indicates the increased local deposition and reduced emission outflow.

Recent advances in understanding the natural Hg emission in China also provide a new opportunity to reassess the Hg outflow from China. X. Wang, Lin, et al. (2016) reevaluated the natural release of Hg^0 from soil, vegetation, and water surfaces using new soil Hg data and updated model schemes with physicochemical parameters reported recently. They found a distinct spatial distribution of estimated Hg emission compared to the data reported by Shetty et al. (2008), despite a similar net natural release quantity at ~460 Mg/year in China. Such a spatial distribution transition could also have an impact on regional model results.

Transport, oxidation, and deposition of atmospheric Hg are highly related to concentrations of other air pollutants (such as SO_2, NO_x, CO, and $PM_{2.5}$; Bo et al., 2016; Hong et al., 2016; Lin & Pehkonen, 1999). Hence, accurate inventories for these pollutants not only provide a good foundation for air quality modeling but also improve model performance for atmospheric Hg modeling. High-resolution (0.25° × 0.25°) regional emission inventory data (M. Li et al., 2015) developed from recent Chinese government-led projects (e.g., Multiresolution Emission Inventory for China) enable new modeling assessments to better understand the chemical transport of atmospheric Hg in a region undergoing rapid emission changes caused by diverging drivers of economic growth and air pollution control implementation.

Finally, a comprehensive evaluation of model results requires the support of field observational data. Since 2012, a coordinated observational network for atmospheric Hg in China had been established within the framework of a "973" project, one of the major competitive scientific projects in China. The project expanded atmospheric Hg monitoring in Mainland China to nine sites using the standard operating procedures and a Quality Assurance/Quality control system of Global Mercury Observation System for full comparability of network observations (Figure 1). There are five sites in remote elevated forest/grassland regions (ALS, CBS, SMS, WLG, and BYBLK) and four sites in suburb/rural regions (DMS, CMD, MYSK, and KXD). For the first time, the concentration and wet deposition observed at these sites become available for a comprehensive evaluation of atmospheric Hg modeling results in the Mainland China region (Fu, Zhang, Yu, et al., 2015). The combination of updated emission inventories and observational data availability warrants new assessment efforts to improve our understanding of Hg biogeochemical cycle in China.

This work aims to reassess the chemical transport and deposition of atmospheric Hg, as well as the outflow of Hg emissions in Mainland China using Community Multiscale Air Quality (CMAQ)-Hg v5.1. The Hg mass budget is estimated under three emission inventory scenarios including anthropogenic and natural Hg emissions, natural-only emissions, and zero emission in a model domain covering the East Asia region. Conclusions are made based on the simulation results, and environmental implications regarding the impact of updated emission data on Hg outflow in Mainland China are discussed.

2. Methods

2.1. Domain and Model Description

The model domain is identical to the one used in Lin et al. (2010). Briefly, the domain is in Lambert conformal projection centered at 34° N and 110° E with 97 × 164 grid cells at a 36-km spatial resolution. It has 14 vertical layers with a 100-hPa pressure level at the domain top. The model configuration and model uncertainty of CMAQ-Hg have been discussed in detail previously (Bieser et al., 2017; Lin et al., 2010, 2007, 2006; Pongprueksa et al., 2008). Briefly, CMAQ v5.1 is based on the CMAQ (Byun, 1999) and modified by Bullock and Brehme (2002), and Gbor et al. (2006), Bash (2010), and Bash et al. (2014) include Hg chemistry, deposition fluxes of GOM and PBM, and the bidirectional flux exchange of GEM between the air and natural surfaces. The current atmospheric Hg chemistry in CMAQ v5.1 is implemented in the cb05tump_ae6_aq mechanism. Since the natural emission data applied in the modeling represent the net natural emission quantity and has

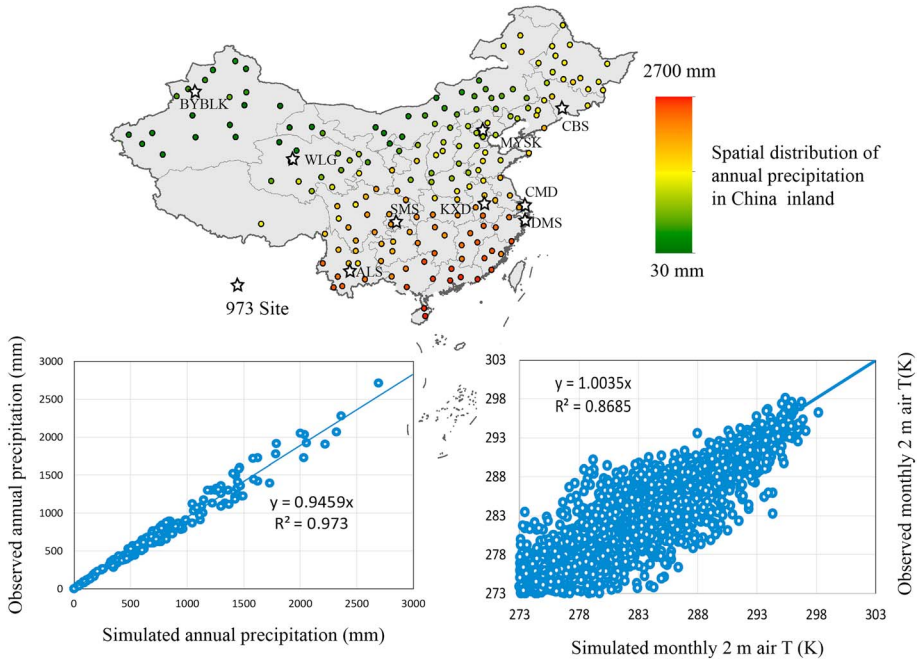

Figure 1. Comparisons of Weather Research and Forecasting simulated precipitation intensity and air temperature at 2-m height versus observed values.

incorporated GEM dry deposition and emission (i.e., net emission = emission from soils + emission from water bodies − uptake by vegetation), the GEM dry deposition module in CMAQ v5.1 was not invoked to avoid double counting of the air-surface exchange of GEM.

Atmospheric redox chemistry of Hg plays an important role in understanding Hg transport and deposition in the atmosphere. However, mechanisms of Hg oxidation in the atmosphere are not well understood, causing uncertainty in the simulation results of Hg chemical transport models (Ariya et al., 2015; Gencarelli et al., 2017; Pacyna et al., 2016; Travnikov et al., 2017; L. M. Zhang et al., 2017). Observational evidence exists that the Br-mediated oxidation pathway plays a dominant role in GEM oxidation in certain atmospheric environments (e.g., the marine boundary, polar regions, and the upper troposphere; Ariya et al., 2015; Gratz et al., 2015; Holmes et al., 2009; Horowitz et al., 2017). However, limited observational data exist with respect to this mechanism and Br concentration in the global atmosphere (Kos et al., 2013; Travnikov et al., 2017). On the other hand, despite questions regarding viability and significance of GEM oxidation mechanisms involving in O_3 and OH (Gratz et al., 2015; Holmes et al., 2010; Horowitz et al., 2017), both theoretical and laboratory studies suggest that these mechanisms can exist in the atmosphere in the presence of aerosol and secondary reactions (Ariya et al., 2015; Feinberg et al., 2015; Gencarelli et al., 2017; Si & Ariya, 2015; Subir et al., 2015; Travnikov et al., 2017). Under polluted conditions in urban areas of China, Hong et al. (2016) suggests that the O_3/OH oxidation pathway dominates GOM formation and that such pathway can be enhanced in the presence of NO_2. Finally, recent model intercomparison studies of the EU Global Mercury Observation System project showed that models with diverse formulations of atmospheric oxidation chemistry are capable of simulating realistic distribution of the GEM concentration and the wet deposition (Bieser et al., 2017; Gencarelli et al., 2017; Pacyna et al., 2016; Travnikov et al., 2017). The chemical schemes based on the O_3- and OH-initiated oxidation in CMAQ-Hg are therefore selected for simulating the chemical transport and Hg deposition in Mainland China, where the lower troposphere has relatively high levels of aerosol and secondary pollutants. The aqueous HO_2 reduction mechanism has been suggested to be unlikely under the oxygenated condition in atmospheric droplets (Gardfeldt & Jonsson, 2003). The aqueous reduction of Hg^{2+} by dicarboxylic acid (such as oxalic acid) was implemented in the aqueous chemistry following the recommendation of Bash et al. (2014). Following Amos et al. (2012), the gas-particle partitioning of Hg (II) was treated as a thermodynamic equilibrium function of local temperature and mass concentration of fine particle matter ($PM_{2.5}$). Although the chemical kinetics and partitioning of Hg in the gaseous and particulate phases under

Table 1
Mercury Emission Inventories (Mg/year) in the Study Domain

Emission inventories	Species	China	Non-China	Total
Anthropogenic emission	Hg^0	278.5	181.2	483.7
	Hg^{2+}	251.2	90.6	305.0
	Hg_p	16.4	30.2	44.3
Natural emission	Hg^0	465.0	248.2	713.2
Total emission		1011.0	550.2	1561.2

such polluted scenarios need to be studied further, model performance evaluation has been conducted to ensure that the model results are representative of observed concentration and wet deposition. With a verified base-case simulation, the relative change of the model results caused by the changes of emission inventory input is assessed in this study.

2.2. Meteorological and Inventory Data

Hour meteorological data are prepared using the Weather Research and Forecasting model version 3.7. Meteorological parameters, including precipitation intensity, air temperature, wind speed, and so on, have a significant influence on the simulation results of atmospheric Hg models (Lin et al., 2007, 2006). Hence, accurate meteorological input data are essential for atmospheric Hg modeling. To obtain the best physics and dynamics options of Weather Research and Forecasting in China, a $L_{25}(5^6)$ orthogonal design of experiments is utilized (supporting information Table S1 and Figure S1). The meteorological physics options were selected based on model evaluation metrics correlation coefficient (R) and root mean square error between simulated results and observed values (e.g., temperature and precipitation intensity) in 750 meteorological stations. The data analysis for the orthogonal design was accomplished using Minitab 16. After the initial L_{25} (5^6) screening, a L_8 (2^4) design was applied to obtain the finally best combination of physics and dynamics options (Table S2 and Figure S2). The selected physics options are Thompson (microphysics options), Betts-Miller-Janjic (cumulus parameterization options), RRTMG (radiation physics options), and BouLac (PBL physics options) based on the results of meteorological model performance evaluation. Figure 1 displays a comparison between simulated annual precipitation and observed values and between simulated air temperature at 2-m height and observed values. The regression slopes (0.95–1.0) and R^2 values (0.87–0.97) suggest that the meteorological input data are representative of the meteorological condition in simulations.

Anthropogenic emission and speciation data in China are based on Wu et al. (2016). The total anthropogenic emission in 2013 is 546 Mg/year, and the emission speciation for $Hg^0/Hg^{2+}/Hg_P$ is 51/46/3 (Wu et al., 2016). The emission inventory outside China is from AMAP/UNEP 2010 (UNEP, 2013). Anthropogenic emission inventory data have a seasonal variation. Overall, 15% of total anthropogenic emissions occur in spring, 20% in summer, 30% in autumn, and 35% in winter (actual variations depend on provinces). Natural emission data are from X. Wang, Lin, et al. (2016), which are derived from the model results of a bidirectional resistant model using the most updated land use in Mainland China (X. Wang, Lin, et al., 2014, 2016). Natural emission outside of China is assumed to equal to the average values from the same land use in China. This is a reasonable assumption because the Hg pollution in entire East Asia and South Asia is relatively high, thus leading to relatively high Hg concentrations in natural surfaces and the derived evasion fluxes (Selin et al., 2008; Strode et al., 2008; X. Wang, Lin, et al., 2016). The total Hg emission quantity utilized in the base-case simulation is 1,561.2 Mg/year (848.0 Mg/year anthropogenic and 713.2 Mg/year natural) in the domain (Table 1). The boundary and initial conditions are regridded from the output of a global 3-D chemical transport model (GEOS-Chem) into the specification of study domain (Song et al., 2015). Other emission data, such as SO_2, NO_x, CO, and so forth, are obtained from Multiresolution Emission Inventory for China (M. Li et al., 2015) and regridded using ArcGIS 10.1 and National Center for Atmospheric Research Command Language.

2.3. Calculation of Regional Mercury Mass Budgets

The methodology of estimating Hg outflow from the domain has been discussed in detail in our earlier works (Lin et al., 2010; Pan et al., 2010). Briefly, the change of Hg mass (*CM*, unit: Mg per season) within the domain during one seasonal simulation period can be calculated as:

$$CM = FM - IM, \tag{1}$$

where *FM* (Mg per season) is the air Hg mass in the domain at the end of the modeling period, and *IM* (Mg) is the initial air Hg mass in the domain. *CM* can be influenced by the Hg mass entering (*InM*, Mg per season) and leaving (*OutM*, Mg per season) the domain through atmospheric transport, emissions from anthropogenic and natural sources in the domain (*EM*, Mg per season), and the wet and dry depositions (*DM*, Mg per season) during one seasonal simulation period. Therefore, the change of Hg mass in the domain also can be calculated as:

$$CM = InM - OutM + EM–DM. \quad (2)$$

Since *InM* and *OutM* represent the Hg mass associated with the atmospheric transport into and out of the study domain, the transport budget (*TB*) can be defined as:

$$TB = OutM–InM. \quad (3)$$

Based equations (1) and (2), the *TB* is also equal to

$$TB = EM–DM - FM + IM. \quad (4)$$

The outflow caused by Hg emissions in the domain (*OF*) is calculated as the difference in *TB* between when there is emission input and when there is no emission input (Lin et al., 2010):

$$OF_i = TB_i - TB_0. \quad (5)$$

Equations (1), (4), and (5) were applied to calculate the *CM*, *TB*, and OF_i in this study, respectively. From the verification in Lin et al. (2010), the OF_i is independent from boundary and initial conditions and represents the actual Hg outflow from the domain. Therefore, we set up three emission scenarios in this study: anthropogenic emission + natural emission input (base case), natural-only emission input (natural-only), and no emission input (zero emission). The simulation was performed from 1 November 2012 to 31 December 2013 (November–December of 2012 as the spin-up time). ArcGIS 10.1 and netCDF Operators were utilized for data retrieval and statistical analysis. These graphic model results were visualized using the Panoply 4 (NASA Goddard Institute for Space Studies).

3. Results

3.1. Predicted Ground Level Atmospheric Hg Concentration and Deposition

The monthly variation of simulated GEM in Mainland China is shown in Figure 2. The simulated annual mean GEM concentration at ground level is 3.0 ± 2.5 ng/m^3, with the highest value (3.4 ± 2.9 ng/m^3) in December and the lowest value (2.6 ± 2.3 ng/m^3) in September. The highest simulated seasonal mean GEM concentration occurs in winter (3.2 ± 2.5 ng/m^3, December–February), followed by autumn (3.0 ± 1.5 ng/m^3, September–November), summer (2.9 ± 1.9 ng/m^3, June–August), and then spring (2.8 ± 1.8 ng/m^3, March–May). The spatial distribution of GEM can be divided by a geodemographic demarcation line, the "Heihe (127.5°E, 50.2°N)-Tengchong (98.5°E, 25.1°N) Line." This imaginary line divides Mainland China as the developed and developing regions. The east side makes up 43% of land area but has 94% of the population (L. Wang, Guixin, et al., 2016). The simulated GEM concentration on the east side of the Heihe-Tengchong Line can be up to 3 times higher than the value on the west side because of the much larger Hg emissions from both anthropogenic and natural sources (X. Wang, Lin, et al., 2016; Wu et al., 2016; L. Zhang, Wang, et al., 2015). A recent review of Hg measurement in China also suggested that the GEM in eastern China ranges from 2.0 to 9.7 ng/m^3, much higher than the 1.5 to 2.5 ng/m^3 GEM in the western China (Fu, Zhang, Yu, et al., 2015). This is consistent with our modeling results.

The simulated PBM concentration ranges from 3 to 493 pg/m^3, with an annual average of 113 ± 76 pg/m^3 (Figure 3). The highest PBM concentration occurs in the regions of northern China, Yangtze River delta, Pearl River Delta, and Sichuan Basin, consistent with higher particulate emissions in these highly industrialized areas (Wu et al., 2016; L. Zhang, Wang, et al., 2015). In contrast to the seasonal variation of GEM, PBM concentration is most elevated in spring (169 ± 57 pg/m^3), followed by autumn (158 ± 46 pg/m^3), winter (69 ± 27 pg/m^3), and then summer (59 ± 31 pg/m^3), as shown in Figure 3. Similar seasonal variations are also observed in field measurement studies (Ci, Zhang, Wang, & Niu, 2011b; Fu, Feng, Sommar, et al., 2012; Fu, Zhang, Yu, et al., 2015). Significantly higher PBM concentration is observed in the regional belt from Xinjiang, inner Mongolia, to northern China in spring (Figure 3). The high PBM concentration mainly reflects the increase of atmospheric particulates caused by the dust storms that occur more frequently in spring. Field observations show that PBM concentration during dust storms is 2–10 times higher than the normal mean values (Y. Q. Zhang, Liu, et al., 2015). Elevated PBM concentration also occurs in the regions of southern,

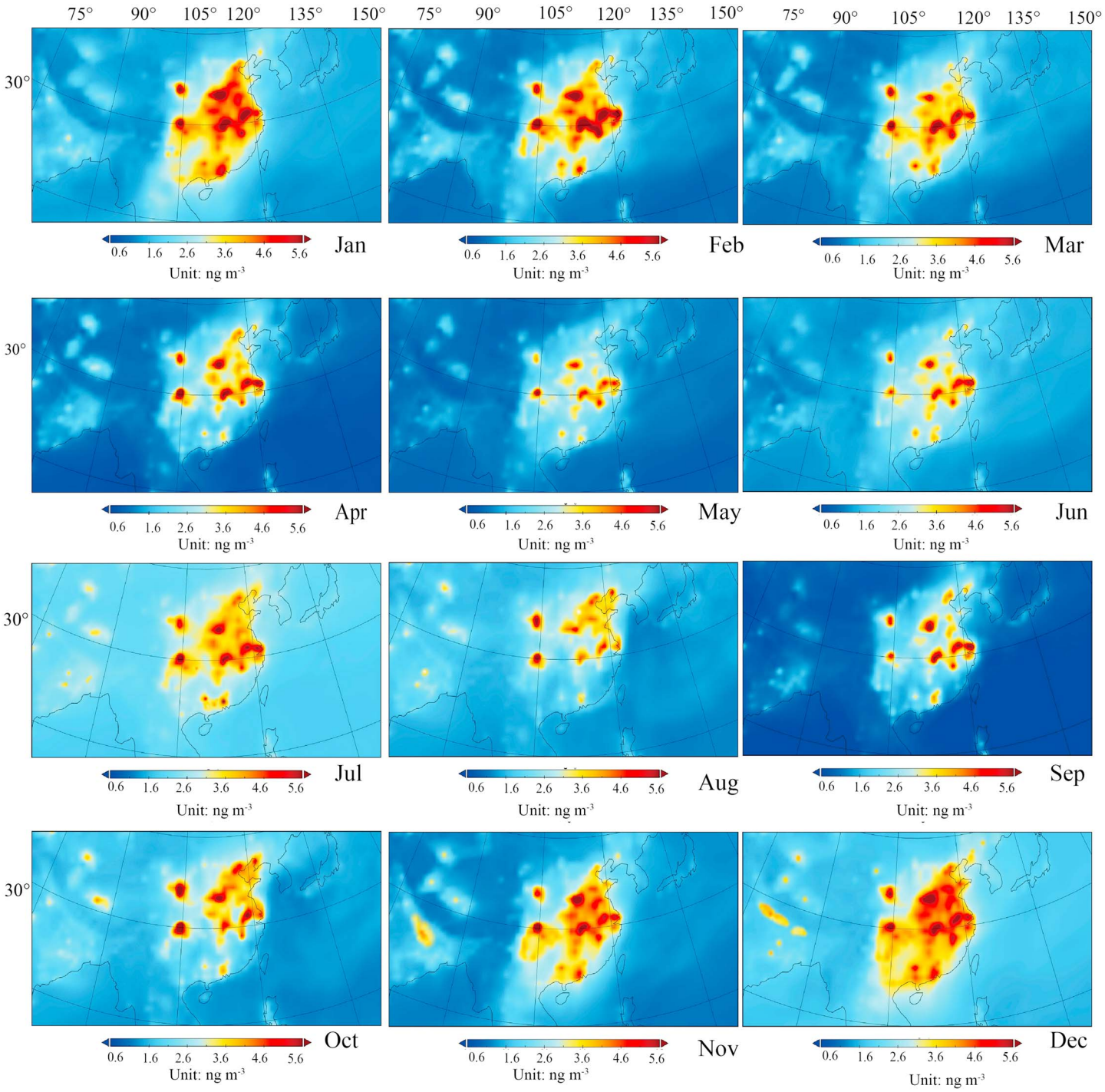

Figure 2. Spatial distribution of simulated monthly mean gaseous elemental mercury concentration at ground level for the base-case simulation.

eastern, and northern China in autumn (Figure 3). This can be attributed to the greater air emissions and the relatively more stable atmosphere in the regions in autumn when regional haze prevails. During this period, the surface wind speed significantly decreases with the weakening of East Asian monsoon (Bo et al., 2016; X. J. Chen et al., 2016; Douglas & Sturm, 2004; Hong et al., 2016), leading to a more stable atmospheric condition and poor pollutant dispersion. Observational data have shown that the PBM concentration during hazy days is 2.6–3.7 times higher than the concentration of nonhazy days (Bo et al., 2016; X. J. Chen et al., 2016; Hong et al., 2016), consistent with our simulation results.

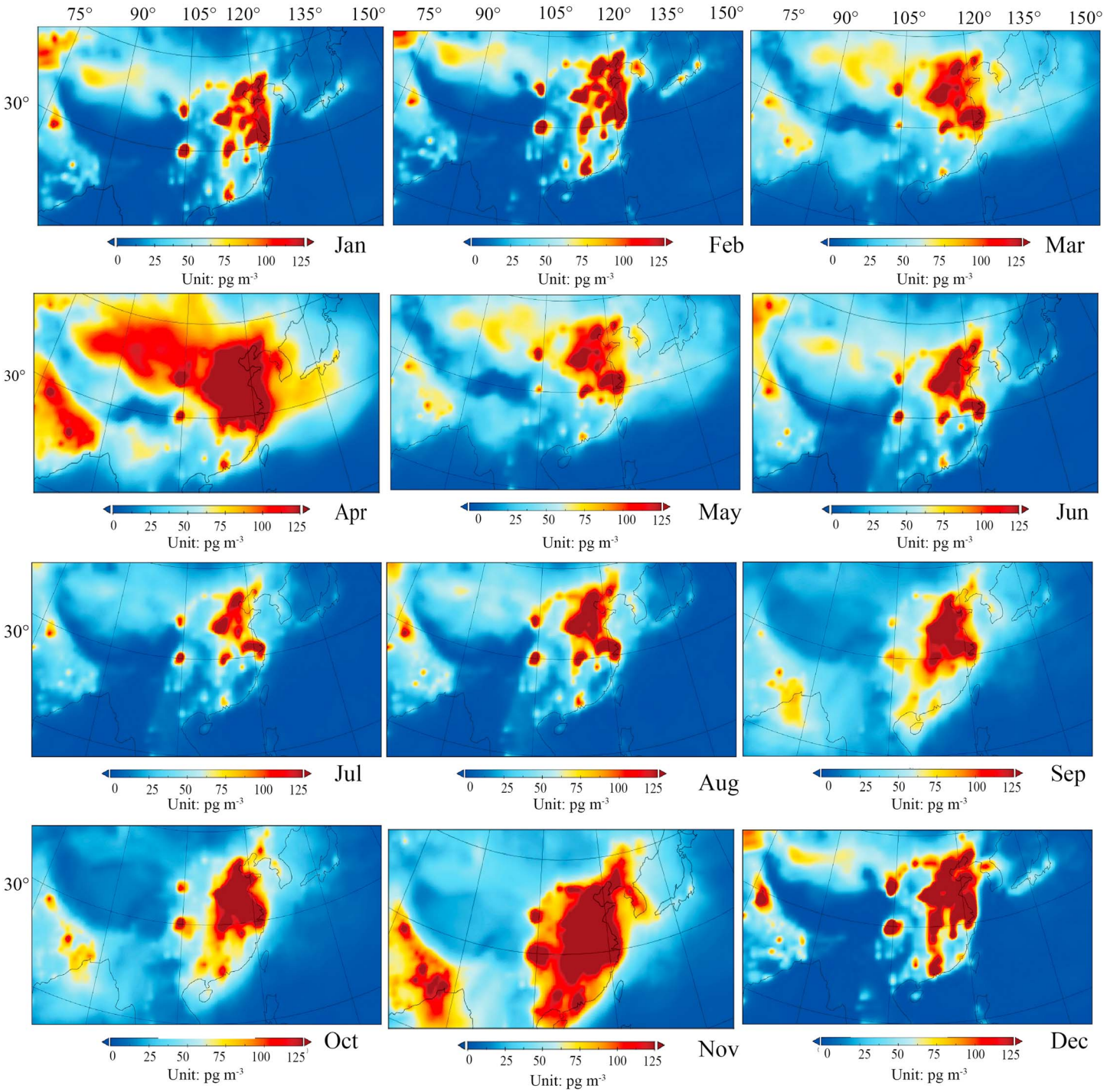

Figure 3. Spatial distribution of simulated monthly mean particulate bound mercury concentration at ground level for the base-case simulation.

The simulated GOM concentration ranges from 1 to 109 pg/m^3, with an annual average of 18 ± 26 pg/m^3 (Figure 4). The spatial distribution of GOM resembles the distribution of primary GOM emission (R^2 = 0.34, $p < 0.01$) since GOM can be readily removed through wet and dry depositions or absorbed onto atmospheric particles (Holloway et al., 2012; Lin & Pehkonen, 1999). The GOM concentration during the rainy seasons (summer and autumn) is 25–30% lower than the level in dry seasons. The simulated GOM concentration in the rainy season (May–October) ranges only from 1 to 18 pg/m^3 in southern China where precipitation is high

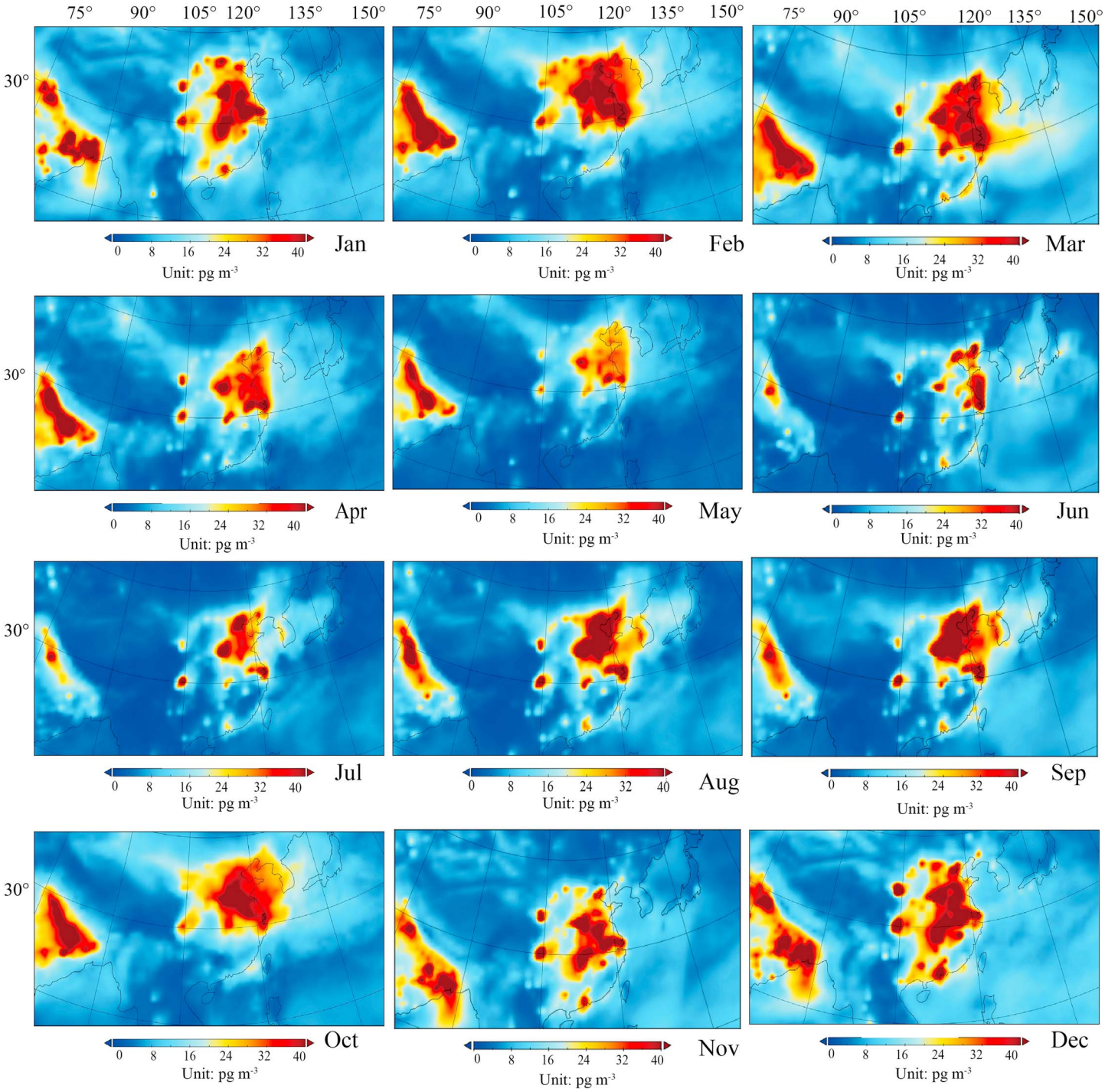

Figure 4. Spatial distribution of simulated monthly mean gaseous oxidized mercury concentration at ground level for the base-case simulation.

(Figure 4), consistent with the 2–25 pg/m^3 GOM observed in these regions (Chand et al., 2008; Fu, Zhang, Yu, et al., 2015; Yu et al., 2015). The simulated PBM concentration is 5–10 times higher than the GOM concentration (Figures 3 and 4). Recent field observations have shown that the PBM concentration can be up to one order of magnitude higher than the GOM concentration (Fu, Zhang, Yu, et al., 2015), consistent with our simulation results. This suggests a significant gas-particle partitioning under the high level of PM concentration.

Table 2
Mercury Mass Balance Budgets Obtained From the Base-Case Simulation

Season	Winter			Spring			Summer			Autumn		
Species	GEM	GOM	PBM	GEM	GOM	PBM	GEM	GOM	PBM	GEM	GOM	PBM
CM	13.0	2.0	1.8	10.4	2.7	6.4	20.1	0.2	0.7	9.4	1.4	10.3
EM	191.6	95.5	6.3	155.1	18.2	1.2	279.3	51	2.7	140.5	65.5	4.3
WD	—	6.5	9	—	8.9	15.9	—	62.4	67.6	—	15	23.5
DD	—	24.6	27.4	—	31.6	32.5	—	11	23.6	—	33.1	29.7
TB	178.6	62.4	−31.9	144.7	−25.1	−53.5	259.2	−32.6	−89.2	131.1	16.0	−59.2
Total	209.1			66.1			147.4			88.0		

Note. CM (Mg per season) is Hg mass accumulation in the atmosphere, EM (Mg per season) is Hg emission in the domain, WD (Mg per season) is wet deposition, DD (Mg per season) is dry deposition, and TB (Mg per season) is transport mass budget. Total is the total transport budget for GEM + GOM + PBM. GEM = gaseous elemental mercury; GOM = gaseous oxidized mercury; PBM = particulate bound mercury.

The simulated annual mean Hg deposition is 36.2 ± 30.4 μg m^{-2} $year^{-1}$, with 15.3 ± 13.2 μg m^{-2} $year^{-1}$ wet deposition and 20.9 ± 17.2 μg m^{-2} $year^{-1}$ dry deposition in Mainland China. The total Hg deposition in the domain is 422 Mg/year with wet deposition accounting for nearly half (49%) of total deposition (Table 2). The deposition has a distinct seasonal pattern with 39% of annual deposition occurring in summer, 24% in autumn, 21% in spring, and 16% in winter. Specifically, the primary emissions of divalent and particulate Hg in northern and eastern China lead to a high level of dry deposition. From the dry (November to April) to the rainy (May to October) season, the total deposition gradually increases with the increasing wet deposition (Figure 5), particularly in southern China. Overall, the wet deposition attributes to 79% of total deposition in summer, 38% in autumn, 28% in spring, and 23% in winter.

3.2. Evaluation of Model Performance Using Base-Case Simulation Results

Figure 6 shows the comparison between the simulations results to observational data collected by the China "973" project Hg ambient monitoring network for the year of 2013. The results are also verified against measurements at the other sites reported in earlier literatures (Figure 7). It should be noted that time periods of measurements reported in earlier literatures are from the year of 2009 to 2014 and not entirely synchronized with the model and emission inventory base year in Figure 7. The atmospheric Hg concentration might have a slight yet statistically insignificant decrease in recent years in China and East Asia (Fu, Zhang, Yu, et al., 2015). However, the reported values are representative of the spatial distribution of atmospheric Hg (Fu, Zhang, Yu, et al., 2015), and model evaluation using these data set provides additional insights of model performance in this study.

Monthly averages of the simulated GEM concentration compare favorably with these observations made by the China "973" project network (all slopes > 0.90; Figure 6). The simulated annual mean GEM concentrations also agree with recently reported field observations ($p = 0.689$, t test, $R^2 = 0.882$, Figure 7). Specifically, the slope of correlation is nearly to 1.0 for observed GEM concentration < 4 ng/m^3. The model results somewhat underestimate for GEM concentration > 4 ng/m^3 (Figure 7). Similarly, the simulated PBM concentrations agree with the observational data at ambient sites where the PBM is <100 pg/m^3 but does not capture the elevated PBM concentration found at highly polluted sites (Figures 6 and 7). The simulated GOM concentrations are poorly correlated to the observed values (Figures 6 and 7) due to the uncertainties in Hg chemistry and GOM measurement (more details in section 4.3), typically 1–3 times higher than the observations. The model estimates of wet deposition agree well with the observed data both for daily and annual levels (Figures 6 and 7).

The underestimation of model results for observed elevated GEM and PBM can be attributed to several reasons. First, the coarse spatial grid resolution (36 km) is not fully capable of producing the instantaneously measured concentration near emission sources (Pongprueksa et al., 2008), which is an inherited limitation of regional modeling analysis. Second, uncertainties in the emission inventory data may also be a factor. For example, Zhao et al. (2015) shows that the uncertainty of Hg emissions from coal-fired power plants ranges −48 to +89% during 2005–2012. Finally, the uncertainties caused by the incomplete understanding

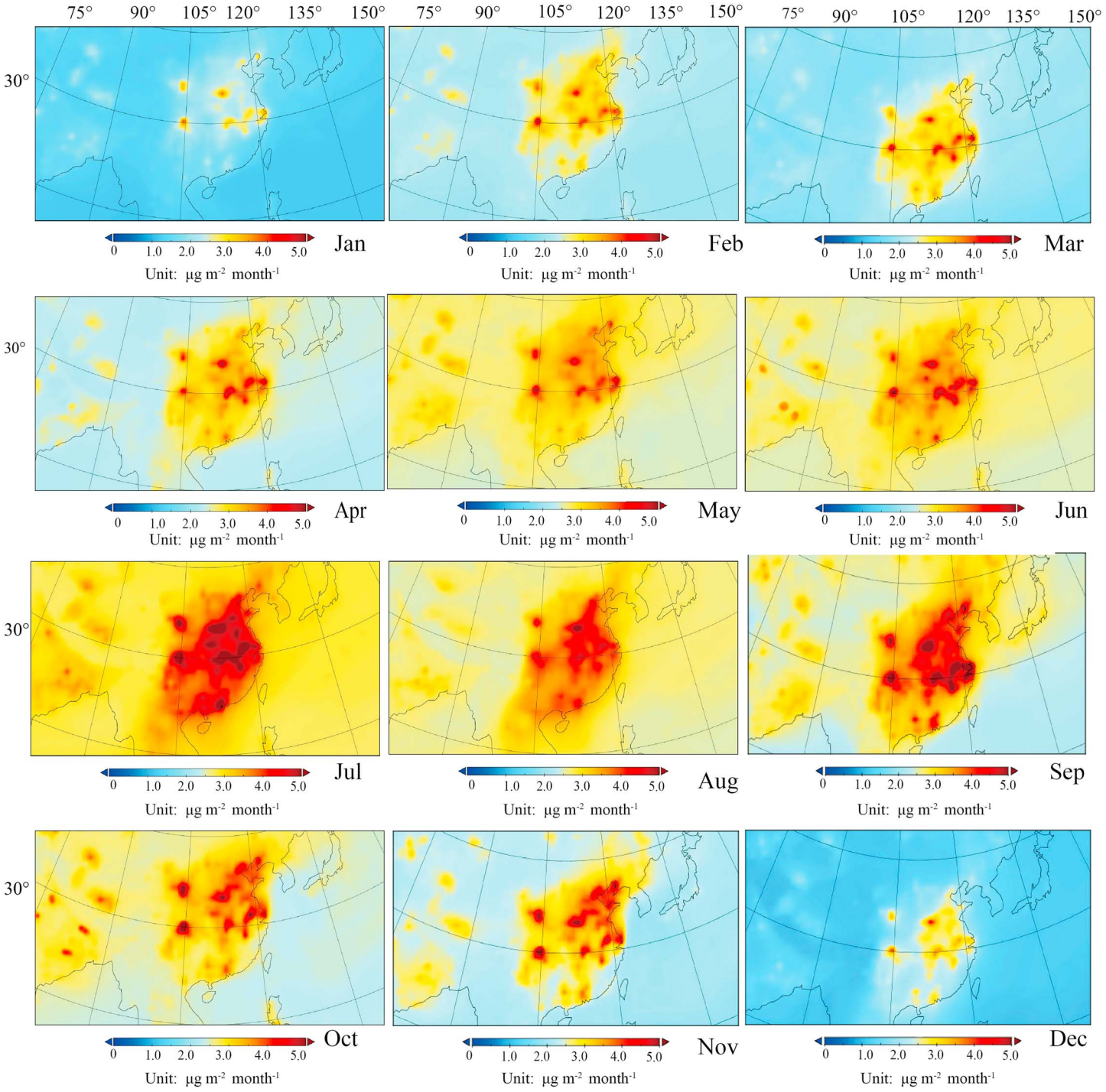

Figure 5. Spatial distribution of simulated total deposition for the base-case simulation.

of Hg redox chemistry and deposition in the atmosphere (Bieser et al., 2017; Gencarelli et al., 2017; Horowitz et al., 2017; Lin et al., 2007, 2006; Pongprueksa et al., 2008; Travnikov et al., 2017) also contribute to the discrepancy between model results and observational data. Nevertheless, the scatterplots of simulated versus observed GEM/PBM concentrations and wet deposition still mostly fall well within the acceptable 0.5–2 slope limit, indicating that the simulation results appropriately capture the magnitude and spatial feature of observations in the domain.

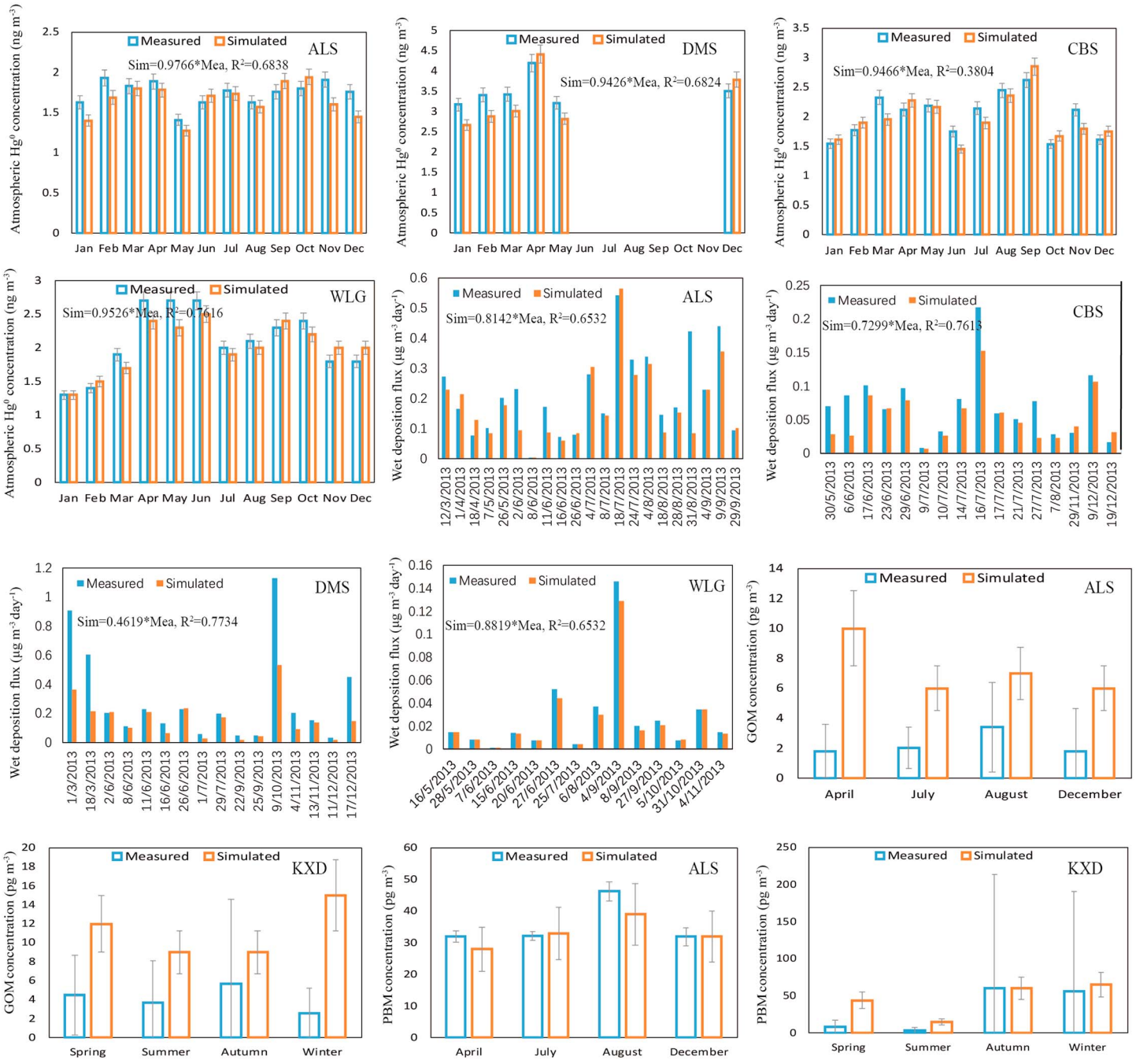

Figure 6. Simulated GEM, wet deposition, GOM, and PBM versus the observed values at "973" project sites in 2013. The site locations have been shown in Figure 1. Sim is the simulated value, and mea is the measured value. Measured GEM concentration and wet deposition at these sites have been reported earlier (Fu, Yang, et al., 2016; Fu, Zhang, Yu, et al., 2015; Hong et al., 2016; Sprovieri et al., 2016; Yu et al., 2015; H. Zhang, Fu, et al., 2016). Because of the limited availability of observational data, the averaging periods for GEM, GOM, PBM, and wet deposition vary. GEM = gaseous elemental mercury; GOM = gaseous oxidized mercury; PBM = particulate bound mercury.

3.3. Atmospheric Hg Mass Budgets

Table 2 and Figure 8 summarize the atmospheric Hg mass budgets in Mainland China. The result shows that the Hg emission and its subsequent chemical transport cause an accumulation of 78 Mg/year in the regional airshed compared to the initial Hg mass in the domain, with 67% of such Hg mass increases attributed to the GEM increase, 8% to the GOM increase, and 25% to the PBM increase. The accumulated Hg mass in the

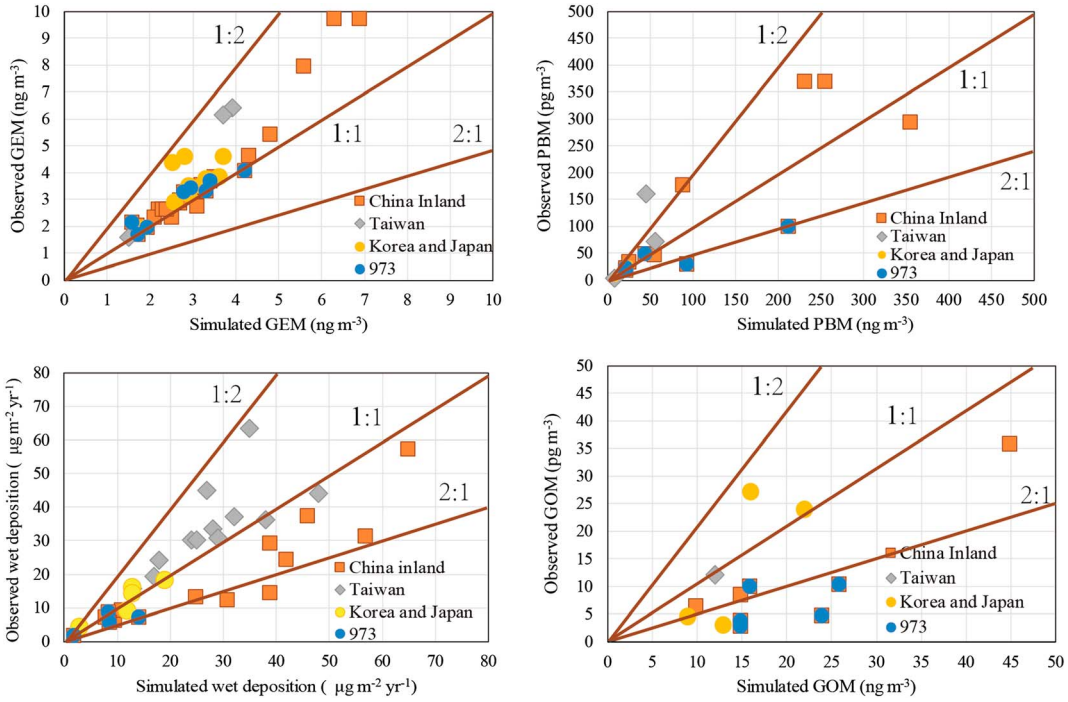

Figure 7. Evaluations of simulated annual GEM, PBM, GOM, and wet deposition for the base case in the domain. The observational data sets obtained from the China "973" mercury ambient monitoring network and from earlier publications for the other sites are all measured during 2009–2014. A more detailed information of measured data set can be found in Table S4 (Bo et al., 2016; H. S. Chen et al., 2015; X. J. Chen et al., 2016; Ci et al., 2015; Ci, Zhang, & Wang, 2011, Ci et al., 2012; Ci, Zhang, Wang, & Niu, 2011a, 2011ab; Friedli et al., 2011; Fu, Feng, Dong, et al., 2010; Fu, Feng, Liang, et al., 2012; Fu, Feng, Shang, et al., 2012; Fu et al., 2011; Fu, Feng, Sommar, et al., 2012; Fu, Feng, Zhu, et al., 2010; Fu, Zhu, et al., 2016; Fu, Yang, et al., 2016; Fu, Zhang, Lin, et al., 2015; Fu, Zhang, Yu, et al., 2015; J.-S. Han et al., 2016; Y.-J. Han et al., 2014; Hong et al., 2016; Huang, Kang, Zhang, et al., 2012; Huang et al., 2013, 2015; Lee et al., 2016; Ma et al., 2016; Ma, Wang, Du, et al., 2015; Ma, Wang, Sun, et al., 2015; Sheu & Lin, 2011, 2013; Sheu et al., 2013, 2010; Song et al., 2015; Tang et al., 2018; Y. M. Wang, Peng, et al., 2014; Weiss-Penzias et al., 2015; Xu et al., 2013, 2015). GEM = gaseous elemental mercury; GOM = gaseous oxidized mercury; PBM = particulate bound mercury.

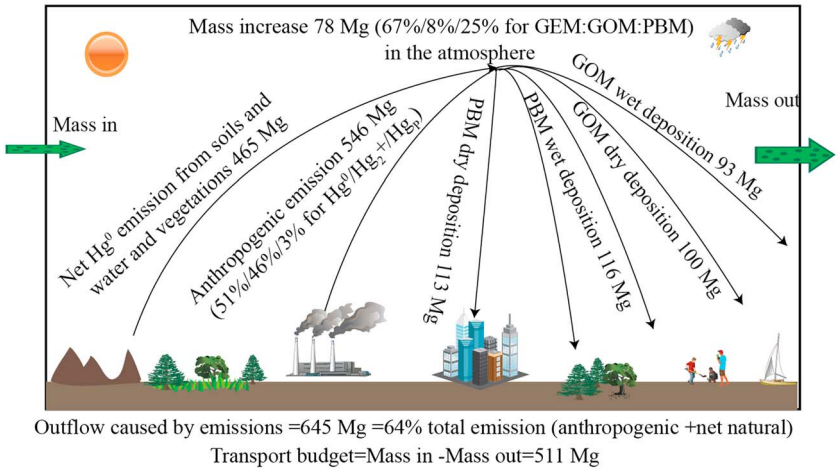

Figure 8. Mass budgets of atmospheric Hg in Mainland China. The "net natural Hg^0 emission" represents the difference between GEM dry deposition and evasion. The transport budget is defined in equation (5). GEM = gaseous elemental mercury; GOM = gaseous oxidized mercury; PBM = particulate bound mercury.

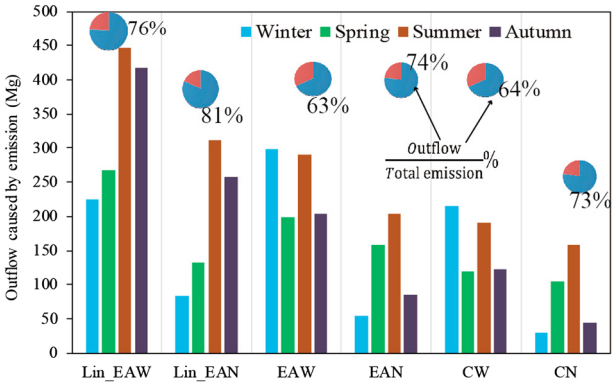

Figure 9. Estimated Hg mass outflows caused by emissions in the domain under various emission scenarios. The pie charts show the ratio of annual outflow over annual total emissions. Lin_EAW and Lin_EAN refer to the base case and the natural-only case in the east Asian domain in Lin et al. (2010), respectively. EAW and EAN are the base case and the natural-only case in the East Asian domain in this study, respectively. CW is the base case and CN is the natural-only case in the mainland China regions in this study.

regional airshed leads to an average increase of approximately 1.0-ng/m^{-3} GEM concentrations at ground level. The accumulation during summer months is higher than in winter because of the stronger natural Hg^0 emission. A substantial quantity of accumulated Hg mass is transported to the upper atmosphere due to the stronger vertical transport, and therefore, the ground-level GEM concentration is lower in summer. The annual deposition of GOM is 193 Mg/year in Mainland China (Table 2 and Figure 8). The annual PBM deposition is 19% higher than the deposition of GOM. We observe a similar seasonal pattern for GOM and PBM depositions. Both GOM and PBM have the highest depositions in summer (38% for GOM and 40% for PBM in Mainland China), followed by autumn (25% for GOM and 23% for PBM), spring (21% for GOM and 21% for PBM), and then winter (16% for GOM and 16% for PBM).

Table 2 shows TBs (equations (3) and (4)) of GEM, GOM, and PBM. The total TB has a distinct seasonal pattern. Winter season has the greatest total TB, followed by summer, autumn, and then spring. GEM is consistently positive in Mainland China. This indicates that there is a net transport of GEM mass out of the region. The transport of GEM is 34% in summer, 26% in winter, 22% in spring, and 18% in autumn; while the TB of GOM and PBM are consistently negative during spring and summer, suggesting a net removal of GOM/PBM from air in the region. These findings are consistent with earlier results by the global models that GEM is the main Hg form exported from East Asia and GOM/PBM deposit locally (L. Chen et al., 2014; H. S. Chen et al., 2015; Selin et al., 2008). The seasonal trend for TB of GEM is mainly caused by seasonal Hg emissions and monsoon shifts in East Asia. The higher TB of GEM in summer than in winter is mainly caused by the much stronger natural Hg^0 emission in summer. The total Hg^0 emission in summer is 1.5 times higher than total emission in winter (Table 2). This TB trend is different from earlier CO and NO_x modeling results that highest export flow over Pacific was observed in winter (Bey et al., 2001; Liu et al., 2003), since the earlier results were caused by the stronger westerlies and a greater emission (e.g., higher emission from biomass burning in Southeast Asia and higher anthropogenic emission in China) in winter (Bey et al., 2001; Liu et al., 2003). Overall, we estimate a net Hg TB of 511 Mg/year from China. When only natural Hg emission is considered, the total deposition decreases by ~40% in Mainland China (Table S3). In the scenario of zero emission, the TB becomes negative (Table S3). With the anthropogenic and natural emissions, the TB shifts from net removal under zero emission scenario to net export. This indicates that Hg emissions in the domain can offset the removal of Hg mass in air coming into the domain and result in Hg mass in air leaving the domain.

Total Hg outflow caused by Hg emissions in the domain under the three emission scenarios using equation (5) is shown in Figure 9. The total Hg emission in Mainland China is 1,011 Mg/year, and the total emission outflow of Hg is 628 Mg/year, accounting for ~63% of total emission. Given the 5,000–6,000 Mg of Hg mass in the atmosphere (Lindberg et al., 2007; Selin et al., 2008), Hg emission total outflow from Mainland China can contribute to approximately 10% of Hg deposition in other regions of the world. Under the natural-only emission scenario, about 73% of natural Hg emission results in outflow. Given the difference of total deposition between the base-case and zero emission case in Tables 2 and S3, it is estimated that ~65% Hg deposition in Mainland China is caused by domestic emissions. This is consistent with these results from L. Chen et al. (2014) and Lin et al. (2010), which exhibits that 60–75% deposition in China is caused by local emissions.

4. Discussion

4.1. Comparison With Previous Model Results

Table 3 shows a summary of results obtained from regional and global scale Hg modeling assessments (L. Chen et al., 2014; H. S. Chen et al., 2015; Jaffe & Strode, 2008; Lin et al., 2010; Pan et al., 2008, 2010; Seigneur et al., 2004; Strode et al., 2008; Travnikov, 2005). It should be noted that most model results are not directly comparable due to differences in emission inventories (particularly natural emissions since earlier studies did not specify the quantity and spatial distribution), Hg chemistry, and model configurations. In

Table 3
Summary of Model Results of Atmospheric Mercury in Mainland China and East Asia Regions

Model	SR	AEI	GO	AO	AR	SC	Model results	Ref
CTM	8 × 10	1,138[a]	OH, O_3, Cl_2	HOCl/OCl^-, OH, O_3	HO_2	1.7–2.1	Asian emissions contribute to 21% of Hg deposition in North America.	1
MSCE-Hem	2.5 × 2.5	1,270[a]	OH, O_3, Cl_2	HOCl/OCl^-, OH, O_3	HO_2	1.5–3.0	Asian anthropogenic emissions contribute to 12% of deposition in Europe, 19% in North America, and 62% in Asia.	2
GEOS-Chem	2.0 × 2.5	1,080[a]	OH, O_3, Cl_2	HOCl/OCl^-, OH, O_3	HO_2	—	1,650 Mg/year of Hg deposition in Asia and West Pacific (65–175°E, 0–60°N), of which 570 Mg/year caused by anthropogenic emissions. Emissions in East Asia contribute to 16% of Hg deposition in North America.	3
GEOS-Chem	4.0 × 5.0	580[a]	OH, O_3, Cl_2	HOCl/OCl^-, OH, O_3	HO_2	—	Asian anthropogenic and natural emissions contribute to 14% and 11% of deposition in North America, respectively.	4
STEM-Hg	1.0 × 1.0	536[b]	OH, O_3, Cl_2, H_2O_2	HOCl/OCl^-, OH, O_3	HO_2	1.4–2.5	702 Mg/year of Hg deposition in East Asia. 342 Mg/year of Asian anthropogenic Hg emission become outflow.	5
CMAQ	36 km × 36 km	826[c]	OH, O_3, Cl_2	HOCl/OCl^-, OH, O_3	HO_2	1.1–9.3	821 Mg/year Hg deposition in East Asia. 75% of the deposition is caused by emissions within the domain. Total emission outflow in the range of 1,300–1,700 Mg/year, representing 70% of the total emissions.	6
STEM-Hg	50 km × 50 km	718[c]	OH, O_3, Cl_2, H_2O_2	HOCl/OCl^-, OH, O_3	HO_2	1.8	1072 Mg/year of Hg deposition in East Asia. 681–714 Mg/year of emissions becomes outflow. 31% of total emissions is deposited within the East Asia domain.	7
GEOS-Chem	2.0 × 2.5	970[a]	Br	Br	—	2.0	380 Mg/year of Hg deposition is in East Asia (not including ocean). Asian emissions cause 10–15% of Hg deposition in Europe, 16–17% in North America, and 64–71% in East Asia.	8
GNAQPMS-Hg	1.0 × 1.0	785[b]	OH, O_3, Cl_2	HOCl/OCl^-, O_3	HO_2	1.4–3.0	Asian anthropogenic emissions contribute to ~3% of deposition in Europe, 4–5% in North America, and 60% in China.	9
CMAQ	36 km × 36 km	546[b]	OH, O_3, Cl_2, H_2O_2	HOCl/OCl^-, OH, O_3	DCA	1.1–8.7	990 Mg/year of total Hg emissions become outflow; of which 645 Mg/year is contributed by emissions in China. 746 Mg/year deposition in East Asia (422 Mg/year in China), 60% of Hg deposition in the East Asia is caused by emission within the domain. The outflow from China causes about 10% of Hg deposition globally.	10

Note. SR is the spatial resolution (latitude × longitude or as noted), AEI is anthropogenic emission inventory (Mg/year), GO is gaseous oxidants, AO is aqueous oxidants, AR is aqueous reductants, and SC is simulated concentration (ng/m^3). The reference of 1 is from Seigneur et al. (2004), 2 from Travnikov (2005), 3 from Jaffe and Strode (2008), 4 from Strode et al. (2008), 5 from Pan et al. (2008), 6 from Lin et al. (2010), 7 from Pan et al. (2010), 8 from L. Chen et al. (2014), 9 from H. S. Chen et al. (2015), and 10 from this study.
[a]Means the domain covering whole Asia. [b]Means East Asia. [c]Means China.

general, regional models produce Hg concentrations more representative of the observed levels in urban and industrial areas. Global model results show that Asian outflow contributes to 16–25% of Hg deposition in North America and 10–15% in the European region, except for one study (H. S. Chen et al., 2015) reporting <5% of contribution in both regions.

The model configurations of CMAQ-Hg in this study and in Lin et al. (2010) are similar, and therefore, it is valuable to compared findings obtained from the two studies. The simulation year of Lin et al. (2010) is 2005. The total annual Hg emission outflow from East Asia estimated in this study is 25% lower than the earlier estimate by Lin et al. (2010; 990 Mg/year in this study versus 1,356/year Mg in Lin et al., 2010) for the East Asia region. It is recognized that the meteorological input data utilized in Lin et al. (2010) and in this study are different, which could have contributed to the difference in the estimated outflows. To rule out this possibility, a separate model simulation was conducted using the 2005 (the model year of Lin et al., 2010) meteorology and the emission inventories in this study. Comparison of the model results obtained by the two sets of meteorological input (Table 4) indicates that the annual difference in outflow caused by interannual variability of meteorology is approximately 5%. Although meteorological variability remains an important factor for the emission outflow quantity, changes in Hg emission quantity, speciation, and spatial/temporal distributions play a more important role in the estimate outflow difference.

Table 4
Contribution of Interannual Variability of Meteorology to the Difference in Estimated Hg Outflows

Difference	January (%)	February (%)	March (%)	April (%)	May (%)	June (%)	July (%)	August (%)	September (%)	October (%)	November (%)	December (%)	Total annual (%)
Wet deposition	12.50	−12.90	5.40	7.10	−14.70	12.00	−10.90	12.50	3.60	−13.50	12.10	−9.50	3.97
Dry deposition	−10.80	14.70	−11.90	8.90	9.40	−14.30	9.70	−9.30	9.65	11.60	−6.80	−7.90	2.65
Outflow	−6.20	7.80	12.10	−10.50	10.80	8.60	−9.45	−6.50	−8.20	−7.90	−9.20	13.30	−5.45

Note. Identical emission data were applied for the two modeling years (2013 and 2005) to assess potential metrological influences. The monthly and annual differences in the resulted chemical transport budgets are calculated as (Case2013 − Case2005) / Case2005 * 100%. Case2013 refers to the model results using 2013 meteorology, and Case2005 refers to the model results using the 2005 meteorology.

The natural emission in Lin et al. (2010) is based on the estimate by Shetty et al. (2008). Lin et al. (2010) estimated that 786 Mg/year of natural emission in the East Asia domain becomes outflow, accounting for 81% of the total natural emission. The estimate obtained in this study is 501 Mg/year, 74% of the total natural emission (Figure 9). Such difference can be attributed to several reasons. One is the difference of the total natural emission quantity. Shetty et al. (2008) estimated the total natural emission in the East Asia domain is 834 Mg/year, while our estimated value is 713 Mg/year. The other is that the spatial distribution of the natural Hg release is significantly different between the two inventories. For example, the natural emission in China from X. Wang, Lin, et al. (2016) exhibits stronger Hg release on the west side of model domain (Figures S3 and S4). Thirty-seven percent of total natural emission in X. Wang, Lin, et al. (2016) is from the west side of the Heihe-Tengchong line, compared to only 11% from the same region in Shetty et al. (2008). The difference in spatial distribution leads to a greater fraction of natural Hg emission deposited or remained in the atmosphere. Since the outflow of Hg emissions in East Asia is mainly driven by the prevailing westerlies, the evaded Hg from the western China has a longer residence time in the domain (X. Wang, Lin, et al., 2016). Finally, the temporal distribution of natural emission also plays an important role. Shetty et al. (2008) estimated 57% natural emission in summer, 19% in spring and autumn, and 5% in winter, in contrast to the 51% in summer, 28% in spring, 13% in autumn, and 8% in winter in this study (X. Wang, Lin, et al., 2016).

The total anthropogenic Hg emission used in this study is also similar to the quantity estimated by Lin et al. (2010; 833 versus 826 Mg/year). However, the speciation of anthropogenic Hg emissions in this study is 51/46/3 for $Hg^0/Hg^{2+}/Hg_P$, different from the 56/32/12 applied in Lin et al. (2010). A larger fraction of oxidized Hg in this study indicates a stronger local deposition. For example, the total deposition of PBM and GOM in this study is 15% higher. Furthermore, Figure 9 shows a smaller Hg outflow to total emission ratio in the base case due to the stronger local deposition of oxidized Hg near the point sources. This highlights the impact of emission speciation change on the quantity of Hg outflow.

4.2. Hg Transport Pattern and Impacts From Anthropogenic and Natural Emissions

The seasonal pattern of GEM concentration exhibiting a winter maximum and autumn minimum is driven by multiple factors including monsoon shifts as well as seasonal variations of anthropogenic and natural emissions (Fu, Zhang, Yu, et al., 2015; Gustin et al., 2015; Mao et al., 2016; L. M. Zhang et al., 2017). The regional air transport is mainly controlled by the westerlies in winter and spring and by the East Asian Monsoon and Indian Monsoon in summer and autumn (Figure S5). Observational and modeling evidence indicated a distinct trans-Pacific transport of Hg from China by the prevailing westerlies (Jaffe et al., 2005; Jaffe & Strode, 2008; Strode et al., 2008). Atmospheric Hg monitoring and receptor modeling results from the China "973" project showed that Hg emissions from biomass burning in South and Southeast Asia can be transported to the southwest region of Mainland China, leading to elevated Hg concentration events (Fu, Zhang, Lin, et al., 2015; X. Wang et al., 2015; H. Zhang, Fu, et al., 2016). Furthermore, Hg observation at Mt. Changbai (a high mountain site in Northeast China) indicated that high-GEM events can be caused by the air masses originating from Korea (Fu, Feng, Shang, et al., 2012).

Mercury emissions applied in this study from natural and anthropogenic sources in China are of similar quantity (465 versus 546 Mg; M. Wang, Chen, et al., 2010; X. Wang, Lin, et al., 2016; Wu et al., 2016), while their seasonal variations and spatial distributions differ significantly. The seasonal change of anthropogenic emission is subject to the variation of industrial activities that peak in winter in China, thus greater Hg anthropogenic emissions in the cold season (S. X. Wang, Zhang, et al., 2010, 2014; Wu et al., 2016). Based on the national

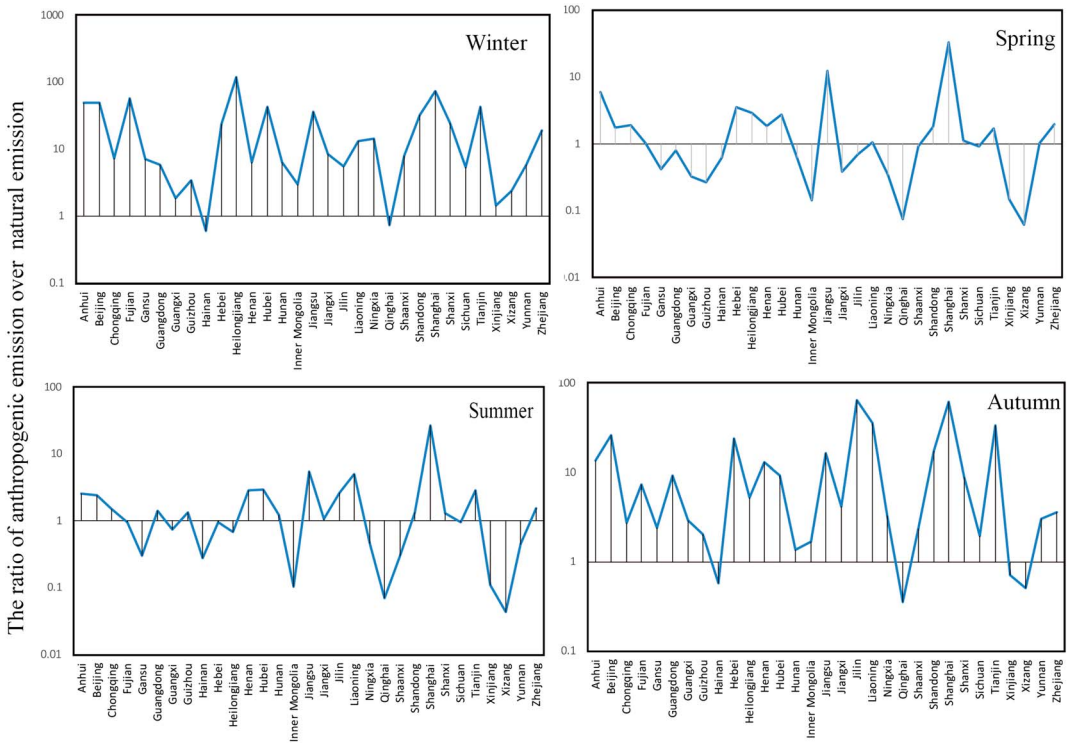

Figure 10. Seasonal ratios of anthropogenic emission over natural emission in Mainland China by province.

statistics, 15% of total anthropogenic emission is assumed in spring, 20% in summer, 30% in autumn, and 35% in winter. The seasonal variation of natural Hg emission mainly depends on land use, farming activities, and meteorology (X. Wang, Lin, et al., 2014, 2016). Half of the natural emission occurs in summer (51%), followed by spring (28%), autumn (13%), and winter (8%; X. Wang, Lin, et al., 2016). For the spatial distribution, anthropogenic sources are concentrated in East China where anthropogenic emission dominates over natural emission (X. Wang, Lin, et al., 2016; Wu et al., 2016). Approximately 70% of anthropogenic Hg emission is from large point sources (L. Zhang, Wang, et al., 2015). Compared to the diffused natural sources, the point-source emissions cause the regionally elevated Hg concentration and deposition in East China. This is reflected by the high GOM, and PBM, and local deposition near these emission sources shown in Figures 3–5.

Figure 10 compares the seasonal emissions from anthropogenic and natural sources by province. The anthropogenic emission dominates the total emission in nearly all provinces in winter and autumn and is the primary driver causing the atmospheric Hg spatial distribution in these seasons (Figure 2). In spring and summer, natural emission can be up to 10 times greater than the anthropogenic emission in less developed regions (e.g., Tibet and Gansu; Figure 10). Due to the relatively weak emission over a large area, natural emission can be further diluted during transport and does not significantly elevate Hg concentration in the provinces of Yunnan, Tibet, and Xinjiang (Figure 2). Strong natural Hg emission driven by the higher temperature in the croplands of northern China (i.e., Hebei and Henan provinces) slightly elevates ambient GEM concentration (Figure 2), consistent with field measurement results (Sommar et al., 2016; X. Wang, Lin, et al., 2016). The simulation results by zeroing out anthropogenic emission ("natural-only" case) show that natural emission causes an increase of 0.3 ng/m^3 annual mean GEM concentration (Table S3). In addition, the simulated Hg deposition in natural-only emission case is ~2 times greater compared to the deposition in the zero-emission case (Table S3), suggesting chemical reactions converting Hg^0 released from natural sources into oxidized Hg in the domain.

It is noteworthy that uncertainties remain in the emission inventories used in this study. The predominant Hg emission sources in China's anthropogenic inventory are coal combustion, nonferrous metal smelting, cement production, and iron and steel production (H. Zhang et al., 2014). Although recent in-stack

Table 5
Hg Chemistry Implemented in this Modeling Assessment Using CMAQ-Hg

Reaction	Rate expression
CMAQ: Gas-phase reactions	cm^3 molecules^{-1} s^{-1}
$Hg^0_{(g)} + O_{3(g)} \rightarrow$ 1/2 GOM + 1/2 PBM	2.11×10^{-18}
$Hg^0_{(g)} + Cl_{2(g)} \rightarrow$ GOM	2.6×10^{-18}
$Hg^0_{(g)} + H_2O_{2(g)} \rightarrow$ GOM	8.5×10^{-19}
$Hg^0_{(g)} + OH_{(g)} \rightarrow$ 1/2 GOM + 1/2 PBM	7.7×10^{-14}
$Hg^0_{(g)} + Cl_{(g)} \rightarrow$ 1/2 GOM + 1/2 $Hg^0_{(g)}$	2.8×10^{-12}
CMAQ: Aqueous-phase reactions	M^{-1} s^{-1}
$Hg^0_{(aq)} + O_{3(aq)} \rightarrow HgO_{(aq)}$	4.7×10^{7}
$HgSO_{3(aq)} \rightarrow Hg^0_{(aq)}$	T exp((31.971–12595)/T) s^{-1}
$Hg(OH)_{2(aq)} + hv \rightarrow Hg^0_{(aq)}$	6.0×10^{-7} cos (solar zenith angle) s^{-1}
$Hg^0_{(aq)} + OH_{(aq)} \rightarrow Hg^{2+}_{(aq)}$	2.0×10^{9}
$Hg^{2+}_{(aq)} + HOCl_{(aq)} \rightarrow Hg^{2+}_{(aq)}$	2.09×10^{6}
$Hg^0_{(aq)} + OCl^-_{(aq)} \rightarrow Hg^{2+}_{(aq)}$	1.99×10^{6}
$Hg^{2+}_{(aq)} + DCAs_{(aq)} \rightarrow Hg^0_{(aq)}$	1.2×10^{4}
GEOS-Chem: Gas-phase reactions	cm^3 molecules^{-1} s^{-1}
$Hg^0_{(g)} + Br_{(g)} + M_{(g)} \rightarrow HgBr_{(g)} + M_{(g)}$	1.46×10^{-32} $(T/298)^{-1.86}$
$HgBr_{(g)} + M \rightarrow Hg^0_{(g)} + M_{(g)} + Br_{(g)}$	1.6×10^{-9} $(T/298)^{-1.86}$ exp (−7801/T)
$HgBr_{(g)} + Br_{(g)} \rightarrow Hg^0_{(g)} + Br_{2(g)}$	3.9×10^{-11}
$HgBr_{(g)} + NO_{2(g)} \rightarrow Hg^0_{(g)} + Br_2NO_{2(g)}$	3.4×10^{-12} (391/T)
$HgBr_{(g)} + Br_{(g)} \rightarrow HgBr_{2(g)}$	3.0×10^{-11}
$HgBr_{(g)} + NO_{2(g)} \rightarrow HgBrNO_{2(g)}$	k_{NO2} (M,T)
$HgBr_{(g)} + Y_{(g)} \rightarrow HgBrY_{(g)}$	kH_{O2} (M,T)
$Hg^0_{(g)} + Cl_{(g)} + M_{(g)} \rightarrow HgCl_{(g)} + M_{(g)}$	2.2×10^{-32} exp(680(1/T-1/298))
$HgCl_{(g)} + Cl_{(g)} \rightarrow Hg^0_{(g)} + Cl_{2(g)}$	1.2×10^{-11} exp(680(−5492/T)
$HgCl_{(g)} + Br_{(g)} \rightarrow HgClBr$	3.0×10^{-11}
$HgCl_{(g)} + NO_{2(g)} \rightarrow HgClNO_{2(g)}$	k_{NO2} (M,T)
$HgCl_{(g)} + Y_{(g)} \rightarrow HgClY_{(g)}$	kH_{O2} (M,T)
GEOS-Chem: Aqueous-phase reactions	M^{-1} s^{-1}
$Hg^0_{(aq)} + O_{3(aq)} \rightarrow HgO_{(aq)}$	4.7×10^{7}
$Hg^{2+}_{(aq)} + HOCl_{(aq)} \rightarrow Hg^{2+}_{(aq)}$	2.09×10^{6}
$Hg^0_{(aq)} + OH_{(aq)} \rightarrow Hg^{2+}_{(aq)}$	2.0×10^{9}
$Hg^{2+}_{(aq)} + hv \rightarrow Hg^0_{(aq)}$	5.2×10^{-2} local photolysis rate (m^3 STP μg^{-1} s^{-1})

Note. The reaction kinetics follow the recommendations of Holloway et al. (2012), Bieser et al. (2014), Bash et al. (2014), and Horowitz et al. (2017). GOM = gaseous oxidized mercury; PBM = particulate bound mercury.

measurements have improved the emission and speciation factors, emission uncertainties remain in the range of −31–58% for Hg^0, −32–69% for Hg^{2+}, and −51–114% for Hg_p (Wu et al., 2016; L. Zhang, Wang, et al., 2015; Zhao et al., 2015). Emissions from processes of treating Hg wastes (e.g., dust recycling during cement production) and from coal combustion for residential heating in rural regions need further improvement (Fu et al., 2011; Streets et al., 2005; L. Zhang, Wang, et al., 2015; Zhao et al., 2015). Finally, the spatiotemporal resolution of the emission data needs to be enhanced for high-resolution modeling assessment (Mao et al., 2016). There are also knowledge gaps among multiscale inventories obtained from different methodologies that need to be addressed (e.g., downscaling versus bottom-up approach; Zhao et al., 2015; Zhong et al., 2016).

Estimates of natural Hg emission have relatively larger uncertainties compared to anthropogenic emission estimates. Earlier assessments reported a ±2,000 Mg/year uncertainty in global natural emission (Pirrone et al., 2010; X. Wang, Lin, et al., 2016) due to limited understanding in the Hg^0 emission processes from environmental surfaces and a lack of soil characterization data with sufficient geospatial coverage and land use activity changes. Although extensive field measurements have established correlations between Hg emission flux and environmental parameters (e.g., soil temperature and solar radiation), fundamental understanding regarding mechanisms and rates of Hg^{2+} reduction in soil, water body, and on the other natural surfaces limits the development of mechanistically robust air-surface Hg^0 exchange models (Agnan et al., 2016; Bash, 2010; Bash et al., 2007; Pirrone et al., 2010; Sprovieri et al., 2010; X. Wang, Lin, et al., 2014, 2016; W. Zhu et al., 2016).

4.3. Uncertainties of Atmospheric Hg Chemistry in CMAQ-Hg

The inaccuracy of the simulated precipitation fields and assumptions made in the cloud scavenging process represent a major uncertainty for simulating Hg wet deposition (Lin et al., 2006). Earlier studies have suggested that the quality of the precipitation fields has the strongest impact on the simulated wet deposition (Bieser et al., 2014; Bullock & Brehme, 2002; Lin et al., 2007). In this study, the simulated precipitation is representative of the rainfall recorded in Mainland China (Figure 1), and the simulated wet deposition also agrees excellently with measurements (Figures 6 and 7). The model estimate shows that 52–64% of Hg wet deposition is contributed by PBM (Table 2), suggesting a high level of PBM exists in rainwater. This is also consistent with observations showing particulate Hg account for 65–90% of total Hg in rainwater samples collected in the "973" project network and at other sites in China (Fu, Yang, et al., 2016; Huang, Kang, Guo, et al., 2012; Huang, Kang, Zhang, et al., 2012; Huang et al., 2013, 2015). CMAQ-Hg calculates PBM deposition in the precipitation by calculating PBM scavenged into cloud with subsequent Hg^{2+}-particulate equilibria in the aqueous phase (Bullock & Brehme, 2002; Lin et al., 2006). The model treatment appears effectively simulate the quantity of wet deposition measured in China.

Figure 7 shows that the simulated GOM has the largest model-observation discrepancies, with model results overestimating the measured GOM by 109% on average. Similar model overestimations of GOM concentration were also reported at 15–380% in earlier studies using CMAQ-Hg (Bieser et al., 2014; Bullock et al., 2008, 2009; Gbor et al., 2006; Gencarelli et al., 2017; Holloway et al., 2012; Lin et al., 2010; Pongprueksa et al., 2008; J. Zhu et al., 2015) and at 80–117% using GEOS-Chem (Amos et al., 2012; Y. Zhang et al., 2012). Several possible reasons can cause such overestimates. One is the undersampling bias caused by the KCl-coated denuders for GOM measurements used in most field campaigns. Several studies

reported that the GOM concentration measured using a denuder system such as the Tekran speciation module (Model 1130) may underestimate the true GOM concentration by a factor of 1.6–12 times depending on the Hg (II) compound (Gustin et al., 2013, 2015). It has also been reported that the current speciation profiles for GOM emission inventories may contribute to the overestimation of GOM simulation (Bieser et al., 2014). Advancement to improve the accuracy of GOM measurements will provide more reliable data for model evaluation.

Another cause is that the knowledge gap in the present understanding of Hg^0 oxidation chemistry in the gaseous phase (L. M. Zhang et al., 2017). The dominant Hg^0 oxidants in the atmosphere by O_3/OH or by Br (details in Table 5) has been a subject of ongoing scientific debates in the past decade. Several theoretical studies suggested that the production of $HgO_{(g)}$, a potential product of the O_3- and OH-initiated oxidation, appears to be unlikely in the gaseous phase (Shepler & Peterson, 2003; Tossell, 2006). However, laboratory experiments and theoretical investigations both suggest that third-body effects and surfaces make these reactions possible in the atmosphere (Ariya et al., 2015; Pal & Ariya, 2004; Snider et al., 2008; Subir et al., 2011, 2012). High concentrations of O_3 and OH are present in the urban and remote atmosphere in China, and therefore, the contribution of O_3- and OH-initiated oxidations should not be ignored. However, their actual contribution to GOM concentration in polluted airsheds needs further studies. Br-initiated oxidations are significantly faster, and their reaction kinetics are considered more reliable (uncertainty of 10^2 for O_3/OH versus 10^1 for Br-initiated oxidations; Horowitz et al., 2017; Subir et al., 2011, 2012). However, there is a large uncertainty in the global concentration distribution of halogens species in the atmosphere, limiting the performance of atmospheric Hg modeling using a global model such as GEOS-Chem (Horowitz et al., 2017; Subir et al., 2011). The present knowledge implies a possibility of more complex Hg chemistry and multiple oxidation pathways occurring concurrently in various parts of the atmosphere (Travnikov et al., 2017), which requires more experimental verification.

5. Conclusion

This study presents the results of a comprehensive modeling assessment of the emission, chemical transport, and deposition of atmospheric Hg in Mainland China. It is shown that the spatial distribution and temporal variation of atmospheric Hg concentration in China is controlled by the variation of Hg emission and monsoon shifts in different seasons. Elevated levels of aerosol and secondary air pollutants significantly enhance the GOM and PBM concentrations. For example, the spring dust storms and autumn regional haze events are both important causes for the high level of simulated PBM concentration. The emission and chemical transport of Hg result in an accumulation of 78 Mg/year of Hg in the regional airshed of Mainland China, causing an average increase of 1.0 ng/m^3 in atmospheric Hg concentration at ground level, consistent with the recent ground network observations. The outflow of GEM mass is mainly caused by the seasonal Hg emissions and monsoon shifts. Overall, the total Hg deposition in China is estimated to be 422 Mg/year (49% by wet deposition), and ~2/3 of the deposition is caused by domestic emissions. The net Hg transport budget from China is estimated to be 511 Mg/year. Our reassessment on the emission-caused outflow in the East Asia region points to approximately 25% decrease compared to the previous estimate by Lin et al. (2010). Such decrease is mainly caused by changes in Hg emission quantity, speciation, and spatial/temporal distributions.

The primary uncertainties in this modeling assessment are from emission inventories and possibly the inadequate representation of atmospheric Hg chemistry implemented in models. The model does not adequately capture the transient high-level of GEM and PBM concentrations in urban areas. Model results also do not fully explain the seasonal GEM variation in the rural regions of western and northern China. The model overestimation of GOM concentration may be due to the measurement bias caused by GOM sampling using KCl denuders commonly used in automated ground-based monitoring of speciated atmospheric Hg. Continued improvement in the estimates of anthropogenic emission from residential coal combustion and Hg waste treatment processes in China, as well as in natural emission inventory through better understanding of Hg^0 evasion processes from soil, water, and other natural surfaces, will improve future modeling assessment. Fundamental understanding in Hg^0 oxidation mechanisms responsible for Hg removal from the atmosphere will also reduce the uncertainties. Nevertheless, this study provides the current state of understanding on Hg emissions and transport in this emission-intensive region.

Acknowledgments

This work was funded by Chinese Academy of Science through K.C. Wong Education Foundation, and China Postdoctoral Science Foundation (BX201700235 and 2017 M620432), and Opening Fund of the State Key Laboratory of Environmental Geochemistry (SKLEG2017906). The data set used for the modeling evaluation can be found in Table S4, and metalogical data set for the WRF can be found in NCEP ftp (ftp://ftpprd.ncep.noaa.gov/pub/data/nccf/com).

References

Agnan, Y., Le Dantec, T., Moore, C. W., Edwards, G. C., & Obrist, D. (2016). New constraints on terrestrial surface atmosphere fluxes of gaseous elemental mercury using a global database. *Environmental Science & Technology*, *50*(2), 507–524. https://doi.org/10.1021/acs.est.5b04013

Amos, H. M., Jacob, D. J., Holmes, C. D., Fisher, J. A., Wang, Q., Yantosca, R. M., et al. (2012). Gas-particle partitioning of atmospheric Hg (II) and its effect on global mercury deposition. *Atmospheric Chemistry and Physics*, *12*(1), 591–603. https://doi.org/10.5194/acp-12-591-2012

Ariya, P. A., Amyot, M., Dastoor, A., Deeds, D., Feinberg, A., Kos, G., et al. (2015). Mercury physicochemical and biogeochemical transformation in the atmosphere and at atmospheric interfaces: A review and future directions. *Chemical Reviews*, *115*(10), 3760–3802. https://doi.org/10.1021/cr500667e

Bash, J. O. (2010). Description and initial simulation of a dynamic bidirectional air-surface exchange model for mercury in community multiscale air quality (CMAQ) model. *Journal of Geophysical Research*, *115*, D06305. https://doi.org/10.1029/2009JD012834

Bash, J. O., Bresnahan, P., & Miller, D. R. (2007). Dynamic surface interface exchanges of mercury: A review and compartmentalized modeling framework. *Journal of Applied Meteorology and Climatology*, *46*(10), 1606–1618. https://doi.org/10.1175/JAM2553.1

Bash, J. O., Carlton, A. G., Hutzell, W. T., & Bullock, O. R. (2014). Regional air quality model application of the aqueous-phase photo reduction of atmospheric oxidized mercury by dicarboxylic acids. *Atmosphere-Basel*, *5*(1), 1–15.

Bey, I., Jacob, D. J., Logan, J. A., & Yantosca, R. M. (2001). Asian chemical outflow to the Pacific in spring: Origins, pathways, and budgets. *Journal of Geophysical Research*, *106*(D19), 23,097–23,113. https://doi.org/10.1029/2001JD000806

Bieser, J., De Simone, F., Gencarelli, C., Geyer, B., Hedgecock, I., Matthias, V., et al. (2014). A diagnostic evaluation of modeled mercury wet depositions in Europe using atmospheric speciated high-resolution observations. *Environemental Science and Pollution Research*, *21*(16), 9995–10012. https://doi.org/10.1007/s11356-014-2863-2

Bieser, J., Slemr, F., Ambrose, J., Brenninkmeijer, C., Brooks, S., Dastoor, A., et al. (2017). Multi-model study of mercury dispersion in the atmosphere: Vertical and interhemispheric distribution of mercury species. *Atmospheric Chemistry and Physics*, *17*(11), 6925–6955. https://doi.org/10.5194/acp-17-6925-2017

Bo, D. D., Cheng, J. P., Xie, H. Y., Zhao, W. C., Wei, Y. Q., & Chen, X. J. (2016). Mercury concentration in fine atmospheric particles during haze and non-haze days in Shanghai, China. *Atmospheric Pollution Research*, *7*(2), 348–354. https://doi.org/10.1016/j.apr.2015.10.002

Bullock, O. R., Atkinson, D., Braverman, T., Civerolo, K., Dastoor, A., Davignon, D., et al. (2008). The North American Mercury Model Intercomparison Study (NAMMIS): Study description and model-to-model comparisons. *Journal of Geophysical Research*, *113*, D17310. https://doi.org/10.1029/2008JD009803

Bullock, O. R., Atkinson, D., Braverman, T., Civerolo, K., Dastoor, A., Davignon, D., et al. (2009). An analysis of simulated wet deposition of mercury from the North American Mercury Model Intercomparison Study. *Journal of Geophysical Research*, *114*, D08301. https://doi.org/10.1029/2008JD011224

Bullock, O. R., & Brehme, K. A. (2002). Atmospheric mercury simulation using the CMAQ model: Formulation description and analysis of wet deposition results. *Atmospheric Environment*, *36*(13), 2135–2146. https://doi.org/10.1016/S1352-2310(02)00220-0

Byun, D. W. (1999). One-atmosphere dynamics description in the Models-3 Community Multi-scale Air Quality (CMAQ) modeling system. *Advance Air Pollution Series*, *6*, 883–892.

Chand, D., Jaffe, D., Prestbo, E., Swartzendruber, P. C., Hafner, W., Weiss-Penzias, P., et al. (2008). Reactive and particulate mercury in the Asian marine boundary layer. *Atmospheric Environment*, *42*(34), 7988–7996. https://doi.org/10.1016/j.atmosenv.2008.06.048

Chen, H. S., Wang, Z. F., Li, J., Tang, X., Ge, B. Z., Wu, X. L., et al. (2015). GNAQPMS-hg v1.0, a global nested atmospheric mercury transport model: Model description, evaluation and application to trans-boundary transport of Chinese anthropogenic emissions. *Geoscientific Model Development*, *8*(9), 2857–2876. https://doi.org/10.5194/gmd-8-2857-2015

Chen, L., Wang, H. H., Liu, J. F., Tong, Y. D., Ou, L. B., Zhang, W., et al. (2014). Intercontinental transport and deposition patterns of atmospheric mercury from anthropogenic emissions. *Atmospheric Chemistry and Physics*, *14*(18), 10,163–10,176. https://doi.org/10.5194/acp-14-10163-2014

Chen, X. J., Balasubramanian, R., Zhu, Q. Y., Behera, S. N., Bo, D. D., Huang, X., et al. (2016). Characteristics of atmospheric particulate mercury in size-fractionated particles during haze days in Shanghai. *Atmospheric Environment*, *131*, 400–408. https://doi.org/10.1016/j.atmosenv.2016.02.019

Ci, Z. J., Wang, C. J., Wang, Z. W., & Zhang, X. S. (2015). Elemental mercury (Hg(0)) in air and surface waters of the Yellow Sea during late spring and late fall 2012: Concentration, spatial-temporal distribution and air/sea flux. *Chemosphere*, *119*, 199–208. https://doi.org/10.1016/j.chemosphere.2014.05.064

Ci, Z. J., Zhang, X. S., & Wang, Z. W. (2011). Elemental mercury in coastal seawater of Yellow Sea, China: Temporal variation and air-sea exchange. *Atmospheric Environment*, *45*(1), 183–190. https://doi.org/10.1016/j.atmosenv.2010.09.025

Ci, Z. J., Zhang, X. S., & Wang, Z. W. (2012). Enhancing atmospheric mercury research in China to improve the current understanding of the global mercury cycle: The need for urgent and closely coordinated efforts. *Environmental Science & Technology*, *46*(11), 5636–5642. https://doi.org/10.1021/es300137y

Ci, Z. J., Zhang, X. S., Wang, Z. W., & Niu, Z. C. (2011a). Atmospheric gaseous elemental mercury (GEM) over a coastal/rural site downwind of East China: Temporal variation and long-range transport. *Atmospheric Environment*, *45*(15), 2480–2487. https://doi.org/10.1016/j.atmosenv.2011.02.043

Ci, Z. J., Zhang, X. S., Wang, Z. W., & Niu, Z. C. (2011b). Phase speciation of mercury (Hg) in coastal water of the Yellow Sea, China. *Marine Chemistry*, *126*(1–4), 250–255. https://doi.org/10.1016/j.marchem.2011.06.004

De Simone, F., Gencarelli, C. N., Hedgecock, I. M., & Pirrone, N. (2016). A modeling comparison of mercury deposition from current anthropogenic mercury emission inventories. *Environmental Science & Technology*, *50*(10), 5154–5162. https://doi.org/10.1021/acs.est.6b00691

Douglas, T. A., & Sturm, M. (2004). Arctic haze, mercury and the chemical composition of snow across northwestern Alaska. *Atmospheric Environment*, *38*(6), 805–820. https://doi.org/10.1016/j.atmosenv.2003.10.042

Driscoll, C. T., Yan, C., Schofield, C. L., Munson, R., & Holsapple, J. (1994). The mercury cycle and fish in the Adirondack Lakes. *Environmental Science & Technology*, *28*(3), 136A–143A. https://doi.org/10.1021/es00052a003

Feinberg, A. I., Kurien, U., & Ariya, P. A. (2015). The Kinetics of Aqueous Mercury(II) Reduction by Sulfite Over an Array of Environmental Conditions. *Water, Air, & Soil Pollution*, *226*(4), 119. https://doi.org/10.1007/s11270-015-2371-0

Friedli, H. R., Arellano, A. F., Geng, F., Cai, C., & Pan, L. (2011). Measurements of atmospheric mercury in Shanghai during September 2009. *Atmospheric Chemistry and Physics*, *11*(8), 3781–3788. https://doi.org/10.5194/acp-11-3781-2011

Fu, X., Zhu, W., Zhang, H., Sommar, J., Yu, B., Yang, X., et al. (2016). Depletion of atmospheric gaseous elemental mercury by plant uptake at Mt. Changbai, Northeast China. *Atmospheric Chemistry and Physics*, *16*(20), 12,861–12,873. https://doi.org/10.5194/acp-16-12861-2016

Fu, X. W., Feng, X., Dong, Z. Q., Yin, R. S., Wang, J. X., Yang, Z. R., & Zhang, H. (2010). Atmospheric gaseous elemental mercury (GEM) concentrations and mercury depositions at a high-altitude mountain peak in South China. *Atmospheric Chemistry and Physics*, *10*(5), 2425–2437. https://doi.org/10.5194/acp-10-2425-2010

Fu, X. W., Feng, X., Liang, P., Deliger, H., Zhang, J. J., & Liu, P. (2012). Temporal trend and sources of speciated atmospheric mercury at Waliguan GAW station, northwestern China. *Atmospheric Chemistry and Physics*, *12*(4), 1951–1964. https://doi.org/10.5194/acp-12-1951-2012

Fu, X. W., Feng, X., Shang, L. H., Wang, S. F., & Zhang, H. (2012). Two years of measurements of atmospheric total gaseous mercury (TGM) at a remote site in Mt. Changbai area, northeastern China. *Atmospheric Chemistry and Physics*, *12*(9), 4215–4226. https://doi.org/10.5194/acp-12-4215-2012

Fu, X. W., Feng, X. B., Qiu, G. L., Shang, L. H., & Zhang, H. (2011). Speciated atmospheric mercury and its potential source in Guiyang, China. *Atmospheric Environment*, *45*(25), 4205–4212. https://doi.org/10.1016/j.atmosenv.2011.05.012

Fu, X. W., Feng, X. B., Sommar, J., & Wang, S. F. (2012). A review of studies on atmospheric mercury in China. *Science of the Total Environment*, *421*, 73–81.

Fu, X. W., Feng, X. B., Zhu, W. Z., Rothenberg, S., Yao, H., & Zhang, H. (2010). Elevated atmospheric deposition and dynamics of mercury in a remote upland forest of southwestern China. *Environmental Pollution*, *158*(6), 2324–2333. https://doi.org/10.1016/j.envpol.2010.01.032

Fu, X. W., Yang, X., Lang, X. F., Zhou, J., Zhang, H., Yu, B., et al. (2016). Atmospheric wet and litterfall mercury deposition at urban and rural sites in China. *Atmospheric Chemistry and Physics*, *16*(18), 11,547–11,562. https://doi.org/10.5194/acp-16-11547-2016

Fu, X. W., Zhang, H., Lin, C. J., Feng, X. B., Zhou, L. X., & Fang, S. X. (2015). Correlation slopes of GEM/CO, GEM/CO2, and GEM/CH4 and estimated mercury emissions in China, South Asia, the Indochinese peninsula, and Central Asia derived from observations in northwestern and southwestern China. *Atmospheric Chemistry and Physics*, *15*(2), 1013–1028. https://doi.org/10.5194/acp-15-1013-2015

Fu, X. W., Zhang, H., Yu, B., Wang, X., Lin, C. J., & Feng, X. B. (2015). Observations of atmospheric mercury in China: A critical review. *Atmospheric Chemistry and Physics*, *15*(16), 9455–9476. https://doi.org/10.5194/acp-15-9455-2015

Gardfeldt, K., & Jonsson, M. (2003). Is bimolecular reduction of Hg (II) complexes possible in aqueous systems of environmental importance. *The Journal of Physical Chemistry. A*, *107*(22), 4478–4482. https://doi.org/10.1021/jp0275342

Gbor, P. K., Wen, D. Y., Meng, F., Yang, F. Q., Zhang, B. N., & Sloan, J. J. (2006). Improved model for mercury emission, transport and deposition. *Atmospheric Environment*, *40*(5), 973–983. https://doi.org/10.1016/j.atmosenv.2005.10.040

Gencarelli, C. N., Bieser, J., Carbone, F., De Simone, F., Hedgecock, I. M., Matthias, V., et al. (2017). Sensitivity model study of regional mercury dispersion in the atmosphere. *Atmospheric Chemistry and Physics*, *17*(1), 627–643. https://doi.org/10.5194/acp-17-627-2017

Gratz, L. E., Ambrose, J. L., Jaffe, D. A., Shah, V., Jaeglé, L., Stutz, J., et al. (2015). Oxidation of mercury by bromine in the subtropical Pacific free troposphere. *Geophysical Research Letters*, *42*, 10,494–10,502. https://doi.org/10.1002/2015GL066645

Gustin, M. S., Amos, H. M., Huang, J., Miller, M. B., & Heidecorn, K. (2015). Measuring and modeling mercury in the atmosphere: A critical review. *Atmospheric Chemistry and Physics*, *15*(10), 5697–5713. https://doi.org/10.5194/acp-15-5697-2015

Gustin, M. S., Huang, J., Miller, M. B., Peterson, C., Jaffe, D. A., Ambrose, J., et al. (2013). Do we understand what the mercury speciation instruments are actually measuring? Results of RAMIX. *Environmental Science & Technology*, *47*(13), 7295–7306. https://doi.org/10.1021/es3039104

Han, J.-S., Seo, Y.-S., Kim, M.-K., Holsen, T. M., & Yi, S.-M. (2016). Total atmospheric mercury deposition in forested areas in South Korea. *Atmospheric Chemistry and Physics*, *16*(12), 7653–7662. https://doi.org/10.5194/acp-16-7653-2016

Han, Y.-J., Kim, J.-E., Kim, P.-R., Kim, W.-J., Yi, S.-M., Seo, Y.-S., & Kim, S.-H. (2014). General trends of atmospheric mercury concentrations in urban and rural areas in Korea and characteristics of high-concentration events. *Atmospheric Environment*, *94*, 754–764. https://doi.org/10.1016/j.atmosenv.2014.06.002

Holloway, T., Voigt, C., Morton, J., Spak, S. N., Rutter, A. P., & Schauer, J. J. (2012). An assessment of atmospheric mercury in the community multiscale air quality (CMAQ) model at an urban site and a rural site in the Great Lakes region of North America. *Atmospheric Chemistry and Physics*, *12*(15), 7117–7133. https://doi.org/10.5194/acp-12-7117-2012

Holmes, C. D., Jacob, D. J., Corbitt, E. S., Mao, J., Yang, X., Talbot, R., & Slemr, F. (2010). Global atmospheric model for mercury including oxidation by bromine atoms. *Atmospheric Chemistry and Physics*, *10*(24), 12,037–12,057. https://doi.org/10.5194/acp-10-12037-2010

Holmes, C. D., Jacob, D. J., Mason, R. P., & Jaffe, D. A. (2009). Sources and deposition of reactive gaseous mercury in the marine atmosphere. *Atmospheric Environment*, *43*(14), 2278–2285. https://doi.org/10.1016/j.atmosenv.2009.01.051

Hong, Q. Q., Xie, Z., Liu, C., Wang, F., Xie, P., & Kang, H. (2016). Speciated atmospheric mercury on haze and non-haze days in an inland city in China. *Atmospheric Chemistry and Physics*, *16*(21), 13,807–13,821. https://doi.org/10.5194/acp-16-13807-2016

Horowitz, H. M., Jacob, D. J., Zhang, Y. X., Dibble, T. S., Slemr, F., Amos, H. M., et al. (2017). A new mechanism for atmospheric mercury redox chemistry: Implications for the global mercury budget. *Atmospheric Chemistry and Physics*, *17*(10), 6353–6371. https://doi.org/10.5194/acp-17-6353-2017

Huang, J., Kang, S. C., Guo, J. M., Zhang, Q. G., Xu, J. Z., Jenkins, M. G., et al. (2012). Seasonal variations, speciation and possible sources of mercury in the snowpack of Zhadang glacier, Mt. Nyainqentanglha, southern Tibetan plateau. *Science of the Total Environment*, *429*, 223–230. https://doi.org/10.1016/j.scitotenv.2012.04.045

Huang, J., Kang, S. C., Wang, S. X., Wang, L., Zhang, Q. G., Guo, J. M., et al. (2013). Wet deposition of mercury at Lhasa, the capital city of Tibet. *Science of the Total Environment*, *447*, 123–132. https://doi.org/10.1016/j.scitotenv.2013.01.003

Huang, J., Kang, S. C., Zhang, Q. G., Guo, J. M., Sillanpaa, M., Wang, Y. J., et al. (2015). Characterizations of wet mercury deposition on a remote high-elevation site in the southeastern Tibetan plateau. *Environmental Pollution*, *206*, 518–526. https://doi.org/10.1016/j.envpol.2015.07.024

Huang, J., Kang, S. C., Zhang, Q. G., Yan, H. Y., Guo, J. M., Jenkins, M. G., et al. (2012). Wet deposition of mercury at a remote site in the Tibetan plateau: Concentrations, speciation, and fluxes. *Atmospheric Environment*, *62*, 540–550. https://doi.org/10.1016/j.atmosenv.2012.09.003

Jaffe, D., Prestbo, E., Swartzendruber, P., Weiss-Penzias, P., Kato, S., Takami, A., et al. (2005). Export of atmospheric mercury from Asia. *Atmospheric Environment*, *39*(17), 3029–3038. https://doi.org/10.1016/j.atmosenv.2005.01.030

Jaffe, D., & Strode, S. (2008). Sources, fate and transport of atmospheric mercury from Asia. *Environment and Chemistry*, *5*(2), 121–126. https://doi.org/10.1071/EN08010

Kos, G., Ryzhkov, A., Dastoor, A., Narayan, J., Steffen, A., Ariya, P. A., & Zhang, L. (2013). Evaluation of discrepancy between measured and modelled oxidized mercury species. *Atmospheric Chemistry and Physics*, *13*(9), 4839–4863. https://doi.org/10.5194/acp-13-4839-2013

Lee, G.-S., Kim, P.-R., Han, Y.-J., Holsen, T. M., Seo, Y.-S., & Yi, S.-M. (2016). Atmospheric speciated mercury concentrations on an island between China and Korea: Sources and transport pathways. *Atmospheric Chemistry and Physics*, *16*(6), 4119–4133. https://doi.org/10.5194/acp-16-4119-2016

Li, M., Zhang, Q., Kurokawa, J., Woo, J. H., He, K. B., Lu, Z., et al. (2015). MIX: A mosaic Asian anthropogenic emission inventory for the MICS-Asia and the HTAP projects. *Atmospheric Chemistry and Physics Discussions*, *15*(23), 34,813–34,869. https://doi.org/10.5194/acpd-15-34813-2015

Li, P., Du, B. Y., Maurice, L., Laffont, L., Lagane, C., Point, D., et al. (2017). Mercury isotope signatures of methylmercury in rice samples from the Wanshan mercury mining area, China: Environmental implications. *Environmental Science & Technology*, *51*(21), 12,321–12,328. https://doi.org/10.1021/acs.est.7b03510

Lin, C. J., Pan, L., Streets, D. G., Shetty, S. K., Jang, C., Feng, X., et al. (2010). Estimating mercury emission outflow from East Asia using CMAQ-Hg. *Atmospheric Chemistry and Physics*, *10*(4), 1853–1864. https://doi.org/10.5194/acp-10-1853-2010

Lin, C. J., & Pehkonen, S. O. (1999). The chemistry of atmospheric mercury: A review. *Atmospheric Environment*, *33*(13), 2067–2079. https://doi.org/10.1016/S1352-2310(98)00387-2

Lin, C. J., Pongprueks, P., Rusell Bulock, O., Lindberg, S. E., Pehkonen, S. O., Jang, C., et al. (2007). Scientific uncertainties in atmospheric mercury models II: Sensitivity analysis in the CONUS domain. *Atmospheric Environment*, *41*(31), 6544–6560. https://doi.org/10.1016/j.atmosenv.2007.04.030

Lin, C. J., Pongprueksa, P., Lindberg, S. E., Pehkonen, S. O., Byun, D., & Jang, C. (2006). Scientific uncertainties in atmospheric mercury models I: Model science evaluation. *Atmospheric Environment*, *40*(16), 2911–2928. https://doi.org/10.1016/j.atmosenv.2006.01.009

Lindberg, S., Bullock, R., Ebinghaus, R., Engstrom, D., Feng, X. B., Fitzgerald, W., et al. (2007). A synthesis of progress and uncertainties in attributing the sources of mercury in deposition. *Ambio*, *36*(1), 19–33. https://doi.org/10.1579/0044-7447(2007)36[19:ASOPAU]2.0.CO;2

Liu, H. Y., Jacob, D. J., Bey, I., Yantosca, R. M., Duncan, B. N., & Sachse, G. W. (2003). Transport pathways for Asian pollution outflow over the Pacific: Interannual and seasonal variations. *Journal of Geophysical Research*, *108*(D20), 8786. https://doi.org/10.1029/2002JD003102

Ma, M., Wang, D., Sun, T., Zhao, Z., & Du, H. (2015). Forest runoff increase mercury output from subtropical forest catchments: An example from an alpine reservoir in a national nature reserve (southwestern China). *Environemental Science and Pollution Research*, *22*(4), 2745–2756. https://doi.org/10.1007/s11356-014-3549-5

Ma, M., Wang, D. Y., Du, H. X., Sun, T., Zhao, Z., Wang, Y. M., & Wei, S. Q. (2016). Mercury dynamics and mass balance in a subtropical forest, southwestern China. *Atmospheric Chemistry and Physics*, *16*(7), 4529–4537. https://doi.org/10.5194/acp-16-4529-2016

Ma, M., Wang, D. Y., Du, H. X., Sun, T., Zhao, Z., & Wei, S. Q. (2015). Atmospheric mercury deposition and its contribution of the regional atmospheric transport to mercury pollution at a national forest nature reserve, Southwest China. *Environemental Science and Pollution Research*, *22*(24), 20,007–20,018. https://doi.org/10.1007/s11356-015-5152-9

Mao, H. T., Cheng, I., & Zhang, L. M. (2016). Current understanding of the driving mechanisms for spatiotemporal variations of atmospheric speciated mercury: A review. *Atmospheric Chemistry and Physics*, *16*(20), 12,897–12,924. https://doi.org/10.5194/acp-16-12897-2016

Pacyna, J. M., Travnikov, O., De Simone, F., Hedgecock, I. M., Sundseth, K., Pacyna, E. G., et al. (2016). Current and future levels of mercury atmospheric pollution on a global scale. *Atmospheric Chemistry and Physics*, *16*(19), 12,495–12,511. https://doi.org/10.5194/acp-16-12495-2016

Pal, B., & Ariya, P. A. (2004). Gas-phase HO center dot-initiated reactions of elemental mercury: Kinetics, product studies, and atmospheric implications. *Environmental Science & Technology*, *38*(21), 5555–5566. https://doi.org/10.1021/es0494353

Pan, L., Carmichael, G. R., Adhikary, B., Tang, Y. H., Streets, D., Woo, J. H., et al. (2008). A regional analysis of the fate and transport of mercury in East Asia and an assessment of major uncertainties. *Atmospheric Environment*, *42*(6), 1144–1159. https://doi.org/10.1016/j.atmosenv.2007.10.045

Pan, L., Lin, C. J., Carmichael, G. R., Streets, D. G., Tang, Y., Woo, J. H., et al. (2010). Study of atmospheric mercury budget in East Asia using STEM-hg modeling system. *Science of the Total Environment*, *408*(16), 3277–3291. https://doi.org/10.1016/j.scitotenv.2010.04.039

Pirrone, N., Cinnirella, S., Feng, X., Finkelman, R. B., Friedli, H. R., Leaner, J., et al. (2010). Global mercury emissions to the atmosphere from anthropogenic and natural sources. *Atmospheric Chemistry and Physics*, *10*(13), 5951–5964. https://doi.org/10.5194/acp-10-5951-2010

Pongprueksa, P., Lin, C. J., Lindberg, S. E., Jang, C., Braverman, T., Bullock, O. R., et al. (2008). Scientific uncertainties in atmospheric mercury models III: Boundary and initial conditions, model grid resolution, and Hg (II) reduction mechanism. *Atmospheric Environment*, *42*(8), 1828–1845. https://doi.org/10.1016/j.atmosenv.2007.11.020

Seigneur, C., Vijayaraghavan, K., Lohman, K., Karamchandani, P., & Scott, C. (2004). Global source attribution for mercury deposition in the United States. *Environmental Science & Technology*, *38*(2), 555–569. https://doi.org/10.1021/es034109t

Selin, N. E. (2009). Global biogeochemical cycling of mercury: A review. *Annual Review of Environment and Resources*, *34*(1), 43–63. https://doi.org/10.1146/annurev.environ.051308.084314

Selin, N. E., Jacob, D. J., Yantosca, R. M., Strode, S., Jaegle, L., & Sunderland, E. M. (2008). Global 3-D land-ocean-atmosphere model for mercury: Present-day versus preindustrial cycles and anthropogenic enrichment factors for deposition. *Global Biogeochemical Cycles*, *22*, GB2011. https://doi.org/10.1029/2007GB003040

Shepler, B. C., & Peterson, K. A. (2003). Mercury monoxide: A systematic investigation of its ground electronic state. *The Journal of Physical Chemistry. A*, *107*(11), 1783–1787. https://doi.org/10.1021/jp027512f

Shetty, S. K., Lin, C. J., Streets, D. G., & Jang, C. (2008). Model estimate of mercury emission from natural sources in East Asia. *Atmospheric Environment*, *42*(37), 8674–8685. https://doi.org/10.1016/j.atmosenv.2008.08.026

Sheu, G. R., & Lin, N. H. (2011). Mercury in cloud water collected on Mt. bamboo in northern Taiwan during the northeast monsoon season. *Atmospheric Environment*, *45*(26), 4454–4462. https://doi.org/10.1016/j.atmosenv.2011.05.036

Sheu, G. R., & Lin, N. H. (2013). Characterizations of wet mercury deposition to a remote islet (Pengjiayu) in the subtropical Northwest Pacific Ocean. *Atmospheric Environment*, *77*, 474–481. https://doi.org/10.1016/j.atmosenv.2013.05.038

Sheu, G. R., Lin, N. H., Lee, C. T., Wang, J. L., Chuang, M. T., Wang, S. H., et al. (2013). Distribution of atmospheric mercury in northern Southeast Asia and South China Sea during Dongsha experiment. *Atmospheric Environment*, *78*, 174–183. https://doi.org/10.1016/j.atmosenv.2012.07.002

Sheu, G. R., Lin, N. H., Wang, J. L., Lee, C. T., Yang, C. F. O., & Wang, S. H. (2010). Temporal distribution and potential sources of atmospheric mercury measured at a high-elevation background station in Taiwan. *Atmospheric Environment*, *44*(20), 2393–2400. https://doi.org/10.1016/j.atmosenv.2010.04.009

Si, L., & Ariya, P. A. (2015). Photochemical reactions of divalent mercury with thioglycolic acid: Formation of mercuric sulfide particles. *Chemosphere*, *119*, 467–472. https://doi.org/10.1016/j.chemosphere.2014.07.022

Snider, G., Raofie, F., & Ariya, P. A. (2008). Effects of relative humidity and CO(g) on the O_3-initiated oxidation reaction of Hg^0(g): Kinetic & product studies. *Physical Chemistry Chemical Physics*, *10*(36), 5616–5623. https://doi.org/10.1039/b801226a

Sommar, J., Zhu, W., Shang, L. H., Lin, C. J., & Feng, X. B. (2016). Seasonal variations in metallic mercury (Hg-0) vapor exchange over biannual wheat-corn rotation cropland in the North China plain. *Biogeosciences*, *13*(7), 2029–2049. https://doi.org/10.5194/bg-13-2029-2016

Song, S., Selin, N. E., Soerensen, A. L., Angot, H., Artz, R., Brooks, S., et al. (2015). Top-down constraints on atmospheric mercury emissions and implications for global biogeochemical cycling. *Atmospheric Chemistry and Physics*, *15*(12), 7103–7125. https://doi.org/10.5194/acp-15-7103-2015

Sprovieri, F., Pirrone, N., Bencardino, M., D'Amore, F., Carbone, F., Cinnirella, S., et al. (2016). Atmospheric mercury concentrations observed at ground-based monitoring sites globally distributed in the framework of the GMOS network. *Atmospheric Chemistry and Physics Discussions*, 1–32. https://doi.org/10.5194/acp-2016-466

Sprovieri, F., Pirrone, N., Ebinghaus, R., Kock, H., & Dommergue, A. (2010). A review of worldwide atmospheric mercury measurements. *Atmospheric Chemistry and Physics*, *10*(17), 8245–8265. https://doi.org/10.5194/acp-10-8245-2010

Streets, D. G., Hao, J. M., Wu, Y., Jiang, J. K., Chan, M., Tian, H. Z., & Feng, X. B. (2005). Anthropogenic mercury emissions in China. *Atmospheric Environment*, *39*(40), 7789–7806. https://doi.org/10.1016/j.atmosenv.2005.08.029

Strode, S. A., Jaegle, L., Jaffe, D. A., Swartzendruber, P. C., Selin, N. E., Holmes, C., & Yantosca, R. M. (2008). Trans-Pacific transport of mercury. *Journal of Geophysical Research*, *113*, D15305. https://doi.org/10.1029/2007JD009428

Subir, M., Ariya, P. A., & Dastoor, A. P. (2011). A review of uncertainties in atmospheric modeling of mercury chemistry I. Uncertainties in existing kinetic parameters—Fundamental limitations and the importance of heterogeneous chemistry. *Atmospheric Environment*, *45*(32), 5664–5676. https://doi.org/10.1016/j.atmosenv.2011.04.046

Subir, M., Ariya, P. A., & Dastoor, A. P. (2012). A review of the sources of uncertainties in atmospheric mercury modeling II. Mercury surface and heterogeneous chemistry—A missing link. *Atmospheric Environment*, *46*, 1–10. https://doi.org/10.1016/j.atmosenv.2011.07.047

Subir, M., Eltouny, N., & Ariya, P. A. (2015). A surface second harmonic generation investigation of volatile organic compound adsorption on a liquid mercury surface. *RSC Advances*, *5*(30), 23464–23470. https://doi.org/10.1039/C4RA13560A

Tang, Y., Wang, S., Wu, Q., Liu, K., Wang, L., Li, S., et al. (2018). Recent decrease trend of atmospheric mercury concentrations in East China: The influence of anthropogenic emissions. *Atmospheric Chemistry and Physics Discussions*, 1–30. https://doi.org/10.5194/acp-2017-1203

Tossell, J. A. (2006). Calculation of the energetics for the oligomerization of gas phase HgO and HgS and for the solvolysis of crystalline HgO and HgS. *The Journal of Physical Chemistry. A*, *110*(7), 2571–2578. https://doi.org/10.1021/jp056280s

Travnikov, O. (2005). Contribution of the intercontinental atmospheric transport to mercury pollution in the Northern Hemisphere. *Atmospheric Environment*, *39*(39), 7541–7548. https://doi.org/10.1016/j.atmosenv.2005.07.066

Travnikov, O., Angot, H., Artaxo, P., Bencardino, M., Bieser, J., D'Amore, F., et al. (2017). Multi-model study of mercury dispersion in the atmosphere: Atmospheric processes and model evaluation. *Atmospheric Chemistry and Physics*, *17*(8), 5271–5295. https://doi.org/10.5194/acp-17-5271-2017

UNEP (2013). *Global Mercury Assessment 2013: Sources, emissions, releases and environmental transport* (p. 44). Geneva, Switzerland: UNEP Chemicals Branch.

Wang, L., Guixin, W., & Zehem, P. (2016). The robustness of China's migration and Heihe-Tengchong line. *China Population Today*, *8*(4), 39–39.

Wang, M., Chen, S., Li, N., & Ma, Y. (2010). A review on the development and application of nano-scale amendment in remediating polluted soils and waters. *Chinese Journal of Eco-Agriculture*, *18*(2), 434–439. https://doi.org/10.3724/SP.J.1011.2010.00434

Wang, S. X., Zhang, L., Li, G. H., Wu, Y., Hao, J. M., Pirrone, N., et al. (2010). Mercury emission and speciation of coal-fired power plants in China. *Atmospheric Chemistry and Physics*, *10*(3), 1183–1192. https://doi.org/10.5194/acp-10-1183-2010

Wang, S. X., Zhang, L., Wang, L., Wu, Q. R., Wang, F. Y., & Hao, J. M. (2014). A review of atmospheric mercury emissions, pollution and control in China. *Frontiers of Environmental Science & Engineering*, *8*(5), 631–649. https://doi.org/10.1007/s11783-014-0673-x

Wang, X., Lin, C. J., & Feng, X. (2014). Sensitivity analysis of an updated bidirectional air-surface exchange model for elemental mercury vapor. *Atmospheric Chemistry and Physics*, *14*(12), 6273–6287. https://doi.org/10.5194/acp-14-6273-2014

Wang, X., Lin, C. J., Yuan, W., Sommar, J., Zhu, W., & Feng, X. B. (2016). Emission-dominated gas exchange of elemental mercury vapor over natural surfaces in China. *Atmospheric Chemistry and Physics*, *16*(17), 11,125–11,143. https://doi.org/10.5194/acp-16-11125-2016

Wang, X., Zhang, H., Lin, C. J., Fu, X. W., Zhang, Y. P., & Feng, X. B. (2015). Transboundary transport and deposition of Hg emission from springtime biomass burning in the Indo-China peninsula. *Journal of Geophysical Research: Atmospheres*, *120*, 9758–9771. https://doi.org/10.1002/2015JD023525

Wang, Y. M., Peng, Y. L., Wang, D. Y., & Zhang, C. (2014). Wet deposition fluxes of total mercury and methylmercury in core urban areas, Chongqing, China. *Atmospheric Environment*, *92*, 87–96. https://doi.org/10.1016/j.atmosenv.2014.03.059

Weiss-Penzias, P., Amos, H. M., Selin, N. E., Gustin, M. S., Jaffe, D. A., Obrist, D., et al. (2015). Use of a global model to understand speciated atmospheric mercury observations at five high-elevation sites. *Atmospheric Chemistry and Physics*, *15*(3), 1161–1173. https://doi.org/10.5194/acp-15-1161-2015

Wu, Q., Wang, S., Li, G., Liang, S., Lin, C.-J., Wang, Y., et al. (2016). Temporal trend and spatial distribution of speciated atmospheric mercury emissions in China during 1978–2014. *Environmental Science & Technology*, *50*(24), 13,428–13,435. https://doi.org/10.1021/acs.est.6b04308

Xu, L., Chen, J., Yang, L., Niu, Z., Tong, L., Yin, L., & Chen, Y. (2015). Characteristics and sources of atmospheric mercury speciation in a coastal city, Xiamen, China. *Chemosphere*, *119*, 530–539. https://doi.org/10.1016/j.chemosphere.2014.07.024

Xu, L. L., Chen, J. S., Niu, Z. C., Yin, L. Q., & Chen, Y. T. (2013). Characterization of mercury in atmospheric particulate matter in the southeast coastal cities of China. *Atmospheric Pollution Research*, *4*(4), 454–461. https://doi.org/10.5094/APR.2013.052

Yu, B., Wang, X., Lin, C. J., Fu, X. W., Zhang, H., Shang, L. H., & Feng, X. B. (2015). Characteristics and potential sources of atmospheric mercury at a subtropical near-coastal site in East China. *Journal of Geophysical Research: Atmospheres*, *120*, 8563–8574. https://doi.org/10.1002/2015JD023425

Zhang, H., Feng, X. B., & Larssen, T. (2014). Selenium speciation, distribution, and transport in a river catchment affected by mercury mining and smelting in Wanshan, China. *Applied Geochemistry*, *40*, 1–10. https://doi.org/10.1016/j.apgeochem.2013.10.016

Zhang, H., Fu, X. W., Lin, C. J., Shang, L. H., Zhang, Y. P., Feng, X. B., & Lin, C. (2016). Monsoon-facilitated characteristics and transport of atmospheric mercury at a high-altitude background site in southwestern China. *Atmospheric Chemistry and Physics*, *16*(20), 13,131–13,148. https://doi.org/10.5194/acp-16-13131-2016

Zhang, L., Wang, S., Wang, L., Wu, Y., Duan, L., Wu, Q., et al. (2015). Updated emission inventories for speciated atmospheric mercury from anthropogenic sources in China. *Environmental Science & Technology*, *49*(5), 3185–3194. https://doi.org/10.1021/es504840m

Zhang, L. M., Lyman, S., Mao, H. T., Lin, C. J., Gay, D. A., Wang, S. X., et al. (2017). A synthesis of research needs for improving the understanding of atmospheric mercury cycling. *Atmospheric Chemistry and Physics*, *17*(14), 9133–9144. https://doi.org/10.5194/acp-17-9133-2017

Zhang, Y., Jaeglé, L., van Donkelaar, A., Martin, R. V., Holmes, C. D., Amos, H. M., et al. (2012). Nested-grid simulation of mercury over North America. *Atmospheric Chemistry and Physics*, *12*(14), 6095–6111. https://doi.org/10.5194/acp-12-6095-2012

Zhang, Y. Q., Liu, R. H., Wang, Y., Cui, X. Q., & Qi, J. H. (2015). Change characteristic of atmospheric particulate mercury during dust weather of spring in Qingdao, China. *Atmospheric Environment*, *102*, 376–383. https://doi.org/10.1016/j.atmosenv.2014.12.005

Zhang, Y. X., Jacob, D. J., Horowitz, H. M., Chen, L., Amos, H. M., Krabbenhoft, D. P., et al. (2016). Observed decrease in atmospheric mercury explained by global decline in anthropogenic emissions. *Proceedings of the National Academy of Sciences of the United States of America*, *113*(3), 526–531. https://doi.org/10.1073/pnas.1516312113

Zhao, Y., Zhong, H., Zhang, J., & Nielsen, C. P. (2015). Evaluating the effects of China's pollution controls on inter-annual trends and uncertainties of atmospheric mercury emissions. *Atmospheric Chemistry and Physics*, *15*(8), 4317–4337. https://doi.org/10.5194/acp-15-4317-2015

Zhong, H., Zhao, Y., Muntean, M., Zhang, L., & Zhang, J. (2016). A high-resolution regional emission inventory of atmospheric mercury and its comparison with multi-scale inventories: A case study of Jiangsu, China. *Atmospheric Chemistry and Physics*, *16*(23), 15,119–15,134. https://doi.org/10.5194/acp-16-15119-2016

Zhu, J., Wang, T., Bieser, J., & Matthias, V. (2015). Source attribution and process analysis for atmospheric mercury in eastern China simulated by CMAQ-Hg. *Atmospheric Chemistry and Physics*, *15*(15), 8767–8779. https://doi.org/10.5194/acp-15-8767-2015

Zhu, W., Lin, C. J., Wang, X., Sommar, J., Fu, X., & Feng, X. (2016). Global observations and modeling of atmosphere–surface exchange of elemental mercury: A critical review. *Atmospheric Chemistry and Physics*, *16*(7), 4451–4480. https://doi.org/10.5194/acp-16-4451-2016